

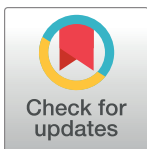
RESEARCH ARTICLE

Regulation of the plastochron by three *many-noded dwarf* genes in barley

Ken-ichiro Hibara¹, Masayuki Miya², Sean Akira Benvenuto², Naoko Hibara-Matsuo¹, Manaki Mimura³, Takanori Yoshikawa⁴, Masaharu Suzuki⁵, Makoto Kusaba⁶, Shin Taketa⁷, Jun-ichi Itoh^{2*}

1 Graduate School of Agricultural Regional Vitalization, Kibi International University, Minamiawaji, Japan, **2** Graduate School of Agricultural and Life Sciences, The University of Tokyo, Tokyo, Japan, **3** National Institute of Genetics, Mishima, Japan, **4** Graduate School of Agriculture, Kyoto University, Kyoto, Japan, **5** Horticultural Sciences Department, University of Florida, Gainesville, Florida, United States of America, **6** Graduate School of Integrated Sciences for Life, Hiroshima University, Higashi-Hiroshima, Japan, **7** Group of Genetic Resources and Functions, Institute of Plant Science and Resources, Okayama University, Kurashiki, Japan

* ajunito@g.ecc.u-tokyo.ac.jp



OPEN ACCESS

Citation: Hibara K-i, Miya M, Benvenuto SA, Hibara-Matsuo N, Mimura M, Yoshikawa T, et al. (2021) Regulation of the plastochron by three *many-noded dwarf* genes in barley. *PLoS Genet* 17(5): e1009292. <https://doi.org/10.1371/journal.pgen.1009292>

Editor: Sarah Hake, "USDA-ARS Pacific West Area", UNITED STATES

Received: December 10, 2020

Accepted: April 6, 2021

Published: May 10, 2021

Copyright: © 2021 Hibara et al. This is an open access article distributed under the terms of the [Creative Commons Attribution License](https://creativecommons.org/licenses/by/4.0/), which permits unrestricted use, distribution, and reproduction in any medium, provided the original author and source are credited.

Data Availability Statement: All relevant data are within the manuscript and its [Supporting Information](#) files, except the genomic sequences of genes appeared in the text. The information of the genes are available by the retrieval tool of DDBJ (<http://getentry.ddbj.nig.ac.jp/>). The accession numbers for the genes are HvPLA2, LC593235; HvPLA3, LC593236; MND4, LC593237; MND1, LC593238; MND8, LC593239; OsBE1, LC593240; OsBE2, LC593241; OsGNAT1, LC593242; and OsGNAT2, LC593243.

Abstract

The plastochron, the time interval between the formation of two successive leaves, is an important determinant of plant architecture. We genetically and phenotypically investigated *many-noded dwarf* (*mnd*) mutants in barley. The *mnd* mutants exhibited a shortened plastochron and a decreased leaf blade length, and resembled previously reported *plastochron1* (*pla1*), *pla2*, and *pla3* mutants in rice. In addition, the maturation of *mnd* leaves was accelerated, similar to *pla* mutants in rice. Several barley *mnd* alleles were derived from three genes—*MND1*, *MND4*, and *MND8*. Although *MND4* coincided with a cytochrome P450 family gene that is a homolog of rice *PLA1*, we clarified that *MND1* and *MND8* encode an N-acetyltransferase-like protein and a MATE transporter-family protein, which are respectively orthologs of rice *GW6a* and maize *BIGE1* and unrelated to *PLA2* or *PLA3*. Expression analyses of the three *MND* genes revealed that *MND1* and *MND4* were expressed in limited regions of the shoot apical meristem and leaf primordia, but *MND8* did not exhibit a specific expression pattern around the shoot apex. In addition, the expression levels of the three genes were interdependent among the various mutant backgrounds. Genetic analyses using the double mutants *mnd4mnd8* and *mnd1mnd8* indicated that *MND1* and *MND4* regulate the plastochron independently of *MND8*, suggesting that the plastochron in barley is controlled by multiple genetic pathways involving *MND1*, *MND4*, and *MND8*. Correlation analysis between leaf number and leaf blade length indicated that both traits exhibited a strong negative association among different genetic backgrounds but not in the same genetic background. We propose that *MND* genes function in the regulation of the plastochron and leaf growth and revealed conserved and diverse aspects of plastochron regulation via comparative analysis of barley and rice.

Funding: This work was supported by a grant from Japan Society for the Promotion of Science, KAKENHI [20H02955 and 20H05406 to JI]. The funders had no role in study design, data collection and analysis, decision to publish, or preparation of the manuscript.

Competing interests: The authors have declared that no competing interests exist.

Author summary

The number of leaves produced during a plant's lifetime is major determinant of plant architecture and affects the efficiency of photosynthesis and crop productivity. The leaf number is dependent on the temporal pattern of leaf initiation at the shoot apical meristem, which is termed the plastochron. The genetic factors involved in plastochron regulation have been identified in several plant species. However, whether the functions of plastochron-related genes and their genetic pathways are universal or diversified among different plant species is unclear. In this study, we investigated *many-noded dwarf* (*mnd*) mutants in barley, which exhibited a shortened plastochron and a decreased leaf blade length. The mutant alleles used in this study were derived from three genes, *MND4*, *MND1*, and *MND8*, which encode a cytochrome P450 family protein, an N-acetyltransferase-like protein, and a MATE transporter-family protein, respectively. Phenotypic and expression analyses revealed that these three MND genes affect the leaf production rate and leaf maturation program, but their expression levels were interdependent. In addition, the plastochron and leaf growth are closely related but independently regulated. We also analyzed the expression patterns and knockout mutants of rice *MND* orthologs to clarify whether their biological functions are conserved in rice and barley. This study provides insight into the genetic mechanisms of plastochron control in grass species.

Introduction

The spatiotemporal pattern of leaf initiation is a major contributor to the formation of plant architecture. The temporal pattern of leaf initiation is termed the plastochron; that is, the time interval between the initiation of two successive leaf primordia. The spatial pattern of leaf initiation along the shoot axis is referred to as phyllotaxy. Both patterns of leaf initiation are determined by the activity of the shoot apical meristem (SAM), which is the source of leaf primordia [1,2]. Although the plastochron and the phyllotaxy are sometimes regulated by shared genetic components operating at the SAM, some genes are specific to one or the other of the patterns [1,3].

PLASTOCHRON1 (*PLA1*) specifically regulates the plastochron in rice (*Oryza sativa*) [4,5]. Loss of function of *PLA1* causes rapidly emerging small leaves, resulting in more than twice the number of leaves compared to the wild type (WT). *PLA1* encodes a plant-specific cytochrome P450 family protein, CYP78A11 [5]. *Arabidopsis KLU* is also a CYP78A-family member and its loss-of-function mutant exhibits accelerated leaf initiation and produces small organs [6]. *PLA2* is another plastochron-regulating factor in rice [7]. *PLA2* encodes a MEI2--like RNA-binding protein, which is an ortholog of *TERMINAL EAR1* (*TE1*) in maize (*Zea mays*) [8]. Although *TE1* plays a role in the regulation of phyllotaxy, accelerated leaf initiation in the loss-of-function mutant is shared between *te1* and *pla2*. *PLA3* has also been reported to regulate the plastochron. A loss-of-function mutant of *PLA3* exhibits not only a shortened plastochron but also pleiotropic phenotypes such as embryonic defects [9]. *PLA3* encodes a homolog of glutamate carboxypeptidase, which dissociates glutamate from small peptides [9]. *PLA3* is the rice ortholog of *Arabidopsis ALTERED MERISTEM PROGRAM1* (*AMP1*) [10] and maize *VIVIPAROUS8* [11]. Consequently, in rice, loss-of-function mutants of three *PLA* genes share the phenotypes of rapid leaf production, small leaf size, and aberrant inflorescence structure [4,7,9].

SQUAMOSA PROMOTER BINDING PROTEIN-LIKE (*SPL*) genes are plant-specific transcription factors, some of which are negatively regulated by *miR156* [12–15]. *SPL* genes are

also involved in plastochron regulation. A double loss-of-function mutant of *AtSPL9* and *AtSPL15* in *Arabidopsis* exhibited a short plastochron [6,16]. Conversely, the expression of an *miR156*-resistant form of *SPL9* caused a prolonged plastochron [6]. In grass species such as rice and maize, *SPL* genes and *miR156* have conserved functions in plastochron regulation. Accumulation of *OsSPL* transcripts caused a prolonged plastochron in rice and loss-of-function mutants of several *SPL* genes and plants overexpressing *miR156* exhibited a short plastochron in both rice and maize [17–23].

The *big embryo1* (*bige1*) mutant in maize exhibits an increased leaf and seminal root number in addition to a large embryo [24]. *BIGE1* encodes a MATE-type transporter that likely plays a role in the secretion of an unidentified small molecule in the trans-Golgi. *BIGE1* function is conserved between maize and *Arabidopsis*, because both single and double mutants of *BIGE1* homologs in *Arabidopsis* produced an increased number of leaves, and the introduction of *BIGE1-GFP* fusion genes into an *Arabidopsis bige1* mutant partially complemented the mutant phenotype [24].

Despite the identification of genes involved in the plastochron, the relationships among these genes and genetic pathways in plastochron regulation are unclear. In *Arabidopsis*, *KLUH/CYP78A5* and *AtSPL9/miR156* affect the plastochron and organ size in parallel genetic pathways [6]. In rice, a *pla1* and *pla2* double mutant exhibited enhanced phenotypes compared with each single mutant, suggesting that *PLA1* and *PLA2* function in independent pathways [7]. Although maize *BIGE1* is involved in the feedback regulation of a *CYP78A* pathway, the phenotypic effect of the interaction on the plastochron has not been elucidated [6]. In addition to the genetic pathways, knowledge of functional conservation of plastochron-related genes among plant species is fragmentary.

Barley (*Hordeum vulgare*) is an important cereal crop for which considerable genetic resources are available, including collections of morphological and developmental mutants [25]. In addition, high-quality genome sequence information is available [26]. Thus, barley is an alternative model for grass molecular genetics with less gene redundancy and is suitable for comparative studies with other grass species. Here, we genetically and phenotypically characterized *many-noded dwarf* (*mnd*) mutants in barley, which were originally described in the 1920s as dwarf mutants with many nodes [27]. All *mnd* mutants exhibited a shortened plastochron, comparable to *pla* mutants in rice. We identified the genes responsible for *mnd* mutants and showed that the plastochron and leaf length are independently controlled by three genetic factors—*MND1*, *MND4*, and *MND8*. Here, we propose to assign a new locus name *mnd8* to a mutation that was found at a locus different from the seven previously described *mnd* loci in barley. We revealed that *MND8* encodes a MATE transporter-family protein, which is an ortholog of maize *BIGE1*. *MND1* encodes an N-acetyltransferase-like protein that reportedly regulates phase changes [28]. *MND4* had been reported as a cytochrome P450-family gene and a homolog of rice *PLA1* [29]. Our phenotypic and genetic analyses of the *mnd* mutants suggested functions for the three *MND* genes and the existence of complex genetic interactions among them. Furthermore, our comparative analysis of rice and barley clarified the diversity and conservation of plastochron genetic pathways.

Results

Plastochron of *mnd* mutants

The *mnd* mutants used in this study are listed in Table 1. Allelism tests revealed that these mutants carried alleles derived from at least three independent genes, *MND1*, *MND4*, and *MND8* (Table 1). *MND4* is also known as *HvMND* [29]. Among the mutants, three—OUM165, OUM169, and OUX051—which are presumed to contain the alleles *mnd8*_{OUM165},

Table 1. *mnd* mutants used in this study.

Strain	Locus name determined by allelism tests	Allele / mutation by sequencing	Mutation effect on protein	Background cultivar
OUM165	<i>mnd8</i>	<i>mnd8.i</i> / T→C	L→P	Akashinriki
OUM166	<i>mnd8</i>	<i>mnd8</i> / G→A	G→N	unknown
OUM168Ku	<i>mnd8</i>	<i>mnd8</i> / G→A	G→N	unknown
OUM169	<i>mnd4</i>	<i>mnd4</i> / G→A	G→D	Akashinriki
OUX051	<i>mnd1</i>	<i>mnd1.a</i> / 8bp insertion	Truncated	Mesa
SM5	<i>mnd1</i>	<i>mnd1</i> / 1bp deletion	Truncated	Kanto Nijo 29
SM6	<i>mnd1</i>	<i>mnd1</i> / 1bp deletion	Truncated	Kanto Nijo 29
GSHO253	<i>mnd1</i>	<i>mnd1</i> / 8bp insertion	Truncated	Mesa
GSHO2038	n.d.	<i>mnd1</i> / 8bp insertion	Truncated	Bowman
GSHO2135	n.d.	<i>mnd4.e</i> / G→A	R→K	Bowman
GSHO1798	<i>mnd4</i>	<i>mnd4.e</i> / G→A	R→K	Akashinriki?
NGB114540	n.d.	<i>mnd1</i> / G→T	R→L	Kristina
NBG114547	n.d.	<i>mnd8</i> / T→A	W→R	Bonus
NGB117205	n.d.	<i>mnd8</i> / G→A	G→E	Bonus

n.d.: not determined. According to the barley gene nomenclature rule, we propose to assign the allele symbols *mnd8.i* to OUM165.

<https://doi.org/10.1371/journal.pgen.1009292.t001>

*mnd4*_{OUM169}, and *mnd1*_{OUX051}, respectively, and Akashinriki, an original cultivar of OUM165 and OUM169, were subjected to detailed genetic and phenotypic analyses.

First, we evaluated the vegetative phenotypes. The three *mnd* mutants produced more leaves than Akashinriki at all stages of vegetative development (Fig 1A–1D). However, the extent of leaf emergence varied among the mutants and growth stages. In the WT and *mnd* mutants, leaf emergence was slow in the early vegetative phase and rapid in the late vegetative phase (Fig 1E). At 40 days after germination, the number of leaves that emerged in *mnd8*_{OUM165} and *mnd1*_{OUX051} was twofold that in the WT, and that in *mnd4*_{OUM169} was intermediate between those of the WT and other mutants, indicating that the three mutants have an increased leaf production rate (Fig 1E).

Two indices represent the temporal pattern of leaf production, the plastochron and the leaf emergence rate which is also referred to as the phyllochron [30]. The plastochron is the time interval between two successive leaves produced at the SAM, and the leaf emergence rate / the phyllochron is the time interval between two successive leaves emerging from the top of the former leaf sheath. Although the plastochron and the leaf emergence rate are equal in rice, the plastochron is shorter than the leaf emergence rate in most other cereal crops [30]. To calculate the plastochron, we observed shoot apices of the WT and three *mnd* mutants at 7 and 14 days after germination (DAG) (S1 Fig). In most shoot apices of Akashinriki at 7 DAG, the P1 primordium was the fifth leaf protruding from the SAM (S1A Fig). At 14 DAG, the P1 primordium was the seventh leaf in most Akashinriki shoot apices (S1E Fig). Therefore, two new leaf primordia were produced from the SAM over 1 week in Akashinriki. In the *mnd* mutants, most of the P1 primordia were fifth leaves at 7 DAG, but eighth leaves at 14 DAG (S1B–S1D and S1F–S1H Fig). The plastochrons of the three *mnd* mutants were shorter than that of the WT (Table 2). We also calculated the leaf emergence rates for the four growth periods. For the first period from 7 to 14 DAG, the leaf emergence rate was longer than the plastochron in the WT and *mnd* mutants. Although the leaf emergence rates in the WT and *mnd* mutants became shorter in the later periods, the difference between the WT and *mnd* mutants increased, suggesting that the leaf production rates of *mnd* mutants increased at later developmental stages. These results suggested that the three *mnd* mutants were defective in plastochron control,

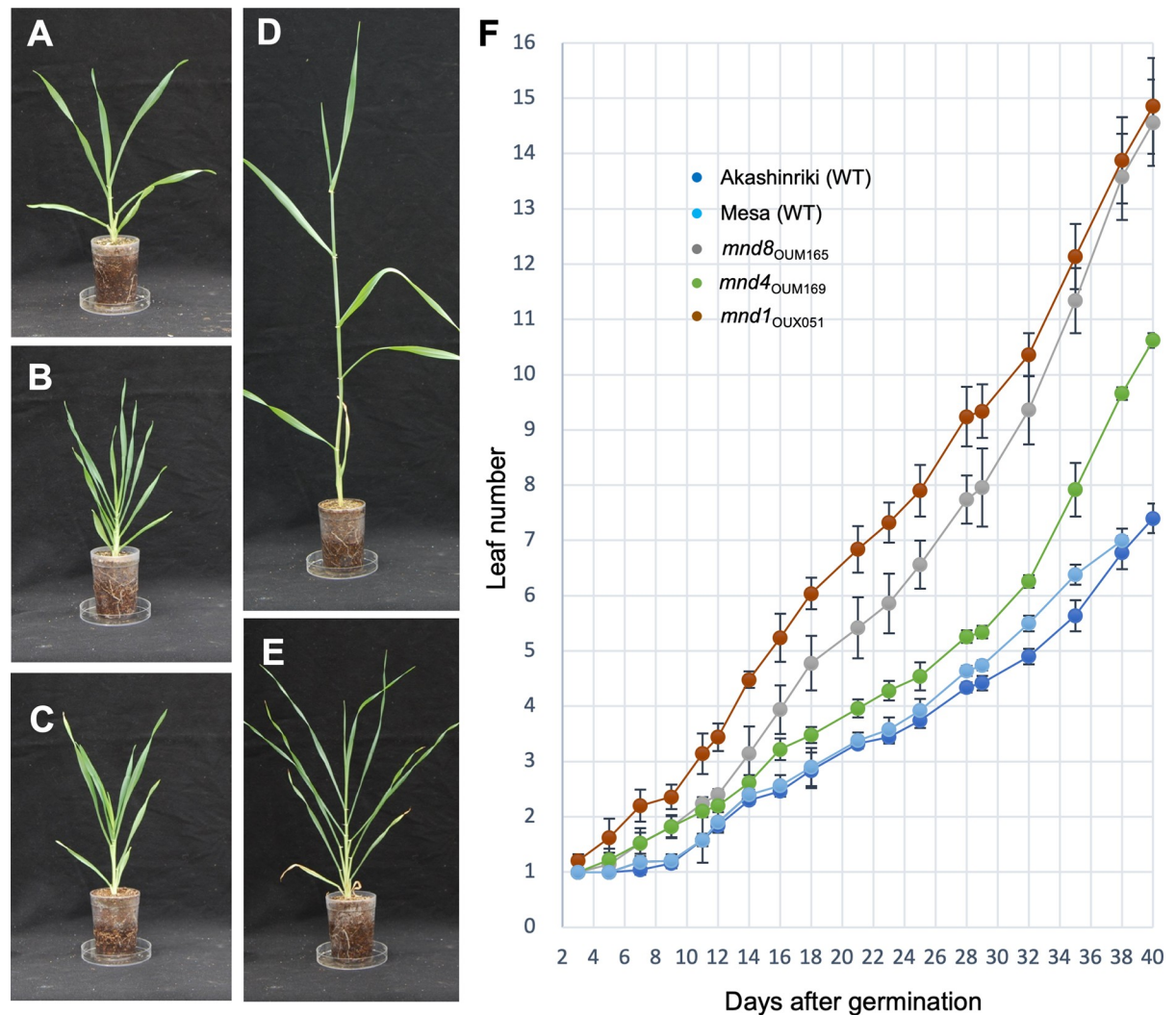


Fig 1. Vegetative phenotypes of *mnd* mutants. (A–E) Seedlings of the wild-type and *mnd* mutants at 1 month after germination. (A) Akashinriki, (B) *mnd8_{OUM165}*, (C) *mnd4_{OUM169}*, (D) Mesa, and (E) *mnd1_{OUX051}*. (F) Changes in leaf number during vegetative development ($n = 5$). Values in F are means \pm SD.

<https://doi.org/10.1371/journal.pgen.1009292.g001>

although the plastochron was shorter than the leaf emergence rate in both the wild-type and *mnd* mutants.

In addition to the vegetative development, the three *mnd* mutants showed abnormal panicle morphology. In the normal panicle of barley, a non-branched single axis of the panicle is produced, but diverged and multiple panicles were observed in *mnd8_{OUM165}* and *mnd1_{OUX051}* (S2 Fig). A panicle abnormality was also recognized in *mnd4_{OUM169}*, which exhibited the weakest vegetative-development phenotype among the *mnd* mutants.

Growth and cell-division pattern of *mnd* leaf primordia

An increased leaf production rate may alter the spatial relationship among leaf primordia in the *mnd* mutants. It is possible that the *mnd* mutants have more leaf primordia inside a leaf primordium than wild type at the same developmental stage. To assess this, we examined the shoot apices of the *mnd* mutants at 14 DAG under an electron microscope (Fig 2). The

Table 2. Characterization of leaf production and leaf emergence rate in *mnd* mutants.

	Akashinriki	<i>mnd8</i> _{OUM165}	<i>mnd4</i> _{OUM169}	<i>mnd1</i> _{OUX051}
Leaf number of P1 stage at 7 DAG ^a	5.0±0.0	5.2±0.4	5.0±0.0	5.8±0.4**
Leaf number of P1 stage at 14 DAG ^a	7.2±0.4	8.0±0.0**	8.0±0.0**	9.2±0.4**
Plastochron during 7–14 DAG (days/leaf production) ^a	3.2±0.7	2.5±0.4**	2.3±0.0**	2.0±0.4**
Phyllochron during 7–14 DAG (days/leaf emergence) ^b	5.6±0.1	4.3±0.6	6.4±0.2	3.0±0.3**
Phyllochron during 14–21 DAG (days/leaf emergence) ^b	6.9±0.1	3.1±0.7**	5.2±0.2**	3.0±0.4**
Phyllochron during 21–28 DAG (days/leaf emergence) ^b	6.9±0.1	3.0±0.7**	5.4±0.2**	2.9±0.7**
Phyllochron during 28–35 DAG (days/leaf emergence) ^b	5.3±0.3	1.9±0.7**	2.6±0.5**	2.4±0.8**

DAG: day after germination.

a: Calculated by the P1 leaf primordium of the shoot sections as shown in [S1 Fig](#).

b: Calculated by the leaf emergence change as shown in [Fig 1F](#). Values are mean±SD, n = 5

**P<0.01 vs. Akashinriki.

<https://doi.org/10.1371/journal.pgen.1009292.t002>

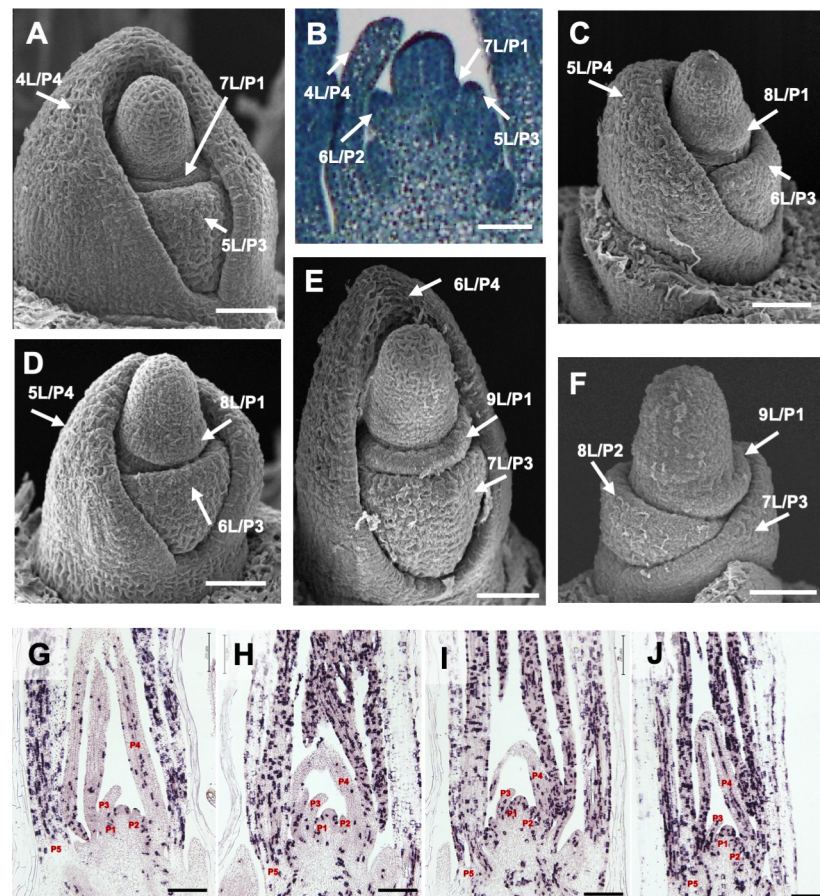


Fig 2. Spatial relationship between leaf-primordium stage and cell-division activity in *mnd* mutants. (A, C–F) Scanning electron micrographs of the shoot apex of Akashinriki and *mnd* mutants at 2 weeks after germination. (A) Shoot apex of Akashinriki. (B) Longitudinal section of the shoot apex of Akashinriki corresponding to (A). Shoot apices in *mnd8*_{OUM165} (C), *mnd4*_{OUM169} (D), and *mnd1*_{OUX051} (E). (F) Shoot apex of *mnd1*_{OUX051} from which the 6L/P4 primordium was removed. xL indicates the xth leaf and Px is the order of leaf emergence from the shoot apical meristem. (G–J) Expression pattern of histone *H4* in the shoot apex of wild-type and *mnd* mutants at 10 days after germination according to *in situ* hybridization. (G) Akashinriki, (H) *mnd8*_{OUM165}, (I) *mnd4*_{OUM169}, and (J) *mnd1*_{OUX051}. Bars: 50 μm in A–F and 200 μm in G–J.

<https://doi.org/10.1371/journal.pgen.1009292.g002>

relationships between successive leaf primordia in the *mnd* mutants were similar to that in the WT. Namely, when the P1 leaf primordium protruded from the flank of the SAM, the P4 leaf primordium gradually enclosed the inner leaf primordia in the WT (Fig 2A and 2B), and this relationship was conserved in the three *mnd* mutants (Fig 2C–2F).

To understand the growth pattern of leaf primordia in the *mnd* mutants, cell division around the shoot apex was investigated by *in situ* hybridization using the cell-division bio-marker histone *H4* (Fig 2G–2J). Patterns of density of histone *H4* signals in the *mnd4* and *mnd8* mutants were similar to that in the WT; namely, cell division activity was relatively low at P1 to P4 and enhanced in P5-stage leaf primordia in the WT, *mnd4*, and *mnd8*. The number of histone *H4* signals in P2 and P3 primordia did not significantly differ among Akashinriki, *mnd4* and *mnd8*, although those of the *mnd1* were increased in P3 (Figs 2G–2J and S3). Therefore, stage-specific developmental events in leaf primordia in the *mnd4* and *mnd8* are likely unchanged, although leaf stage progressions could be more accelerated in the *mnd1*. Thus, the barley *mnd* mutants exhibited rapid leaf production but maintained leaf stage-specific development by rapid leaf maturation, as do *pla* mutants in rice [7].

Molecular identification of three MND genes

The three *mnd* mutants exhibited similar phenotypes, and the affected traits were comparable to those of *pla* mutants in rice. Accordingly, the three *MND* genes in barley could be counterparts of the three rice *PLA* genes [5,7,9].

To identify the three *MND* genes, we first determined the nucleotide sequences of *MND4/HvMND* (HOR5Hr1G081060) in OUM169, a homolog of rice *PLA1* [29] (S4A Fig). We detected a single nucleotide polymorphism between Akashinriki and *mnd4*_{OUM169}. The mutation was a G-to-A single base change (G425A) causing a Gly-to-Asp amino-acid substitution in the first exon of *MND4* (Fig 3A and Table 1). This amino acid is conserved among angiosperms, suggesting it to be responsible for the phenotype of *mnd4*_{OUM169} (S5 Fig). We detected an identical mutation in the other two *mnd* mutants, *mnd4*_{GSHO2135} and *mnd4*_{GSHO1798}, that caused an Arg-to-Lys amino-acid substitution, which has been reported previously as the *mnd4.e* allele [29] (Figs 3A and S5 and Table 1). Because we found multiple *mnd4* alleles linked to a shortened plastochron phenotype, *MND4/HvMND* regulates the plastochron in barley.

Next, to identify candidates for *MND1* and *MND8*, we tested the barley ortholog of *PLA2*: *HvPLA2* (HORVU3Hr1G091930). Rice *pla2* exhibits a phenotype similar to those of barley *mnd* mutants [7]. We determined the nucleotide sequences of *HvPLA2* in various *mnd* mutant and WT pairs. A database search showed that *HvPLA2* is located in barley chromosome 3H, which is syntenic to rice chromosome 1 carrying *PLA2*, but our mapping showed that *MND8* and *MND1* are located on chromosomes 7H and 5H, respectively (S6 Fig). We found no mutation causing an amino-acid change or frameshift in *HvPLA2* in *mnd8*_{OUM165} and *mnd1*_{OUX051}, suggesting that neither *MND8* nor *MND1* is *HvPLA2* (S7 Fig).

A barley ortholog of rice *pla3* was next investigated because of its similar phenotype [9]. The barley ortholog *HvPLA3* (HORVU5Hr1G103900) of *PLA3* in rice chromosome 3, is located on syntenic chromosome 5H. We mapped *MND8* to the distal region of the long arm of barley chromosome 5H (S6 Fig), but this position deviated distally from the *HvPLA3* candidate interval. No mutation was detected in the nucleotide sequence of *HvPLA3* in *mnd8*_{OUM165}. Sequencing of *HvPLA3* in *mnd1*_{OUX051} revealed two point mutations causing amino-acid substitutions, and a six-base deletion causing two amino-acid deletions in *HvPLA3* in *mnd1*_{OUX051}. Although one of the point mutations and the deletion mutation did not change the amino acids conserved among angiosperms, a C-to-A point mutation (C773A) in the first exon caused a Pro-to-Gln amino-acid substitution (P258Q) at a conserved position

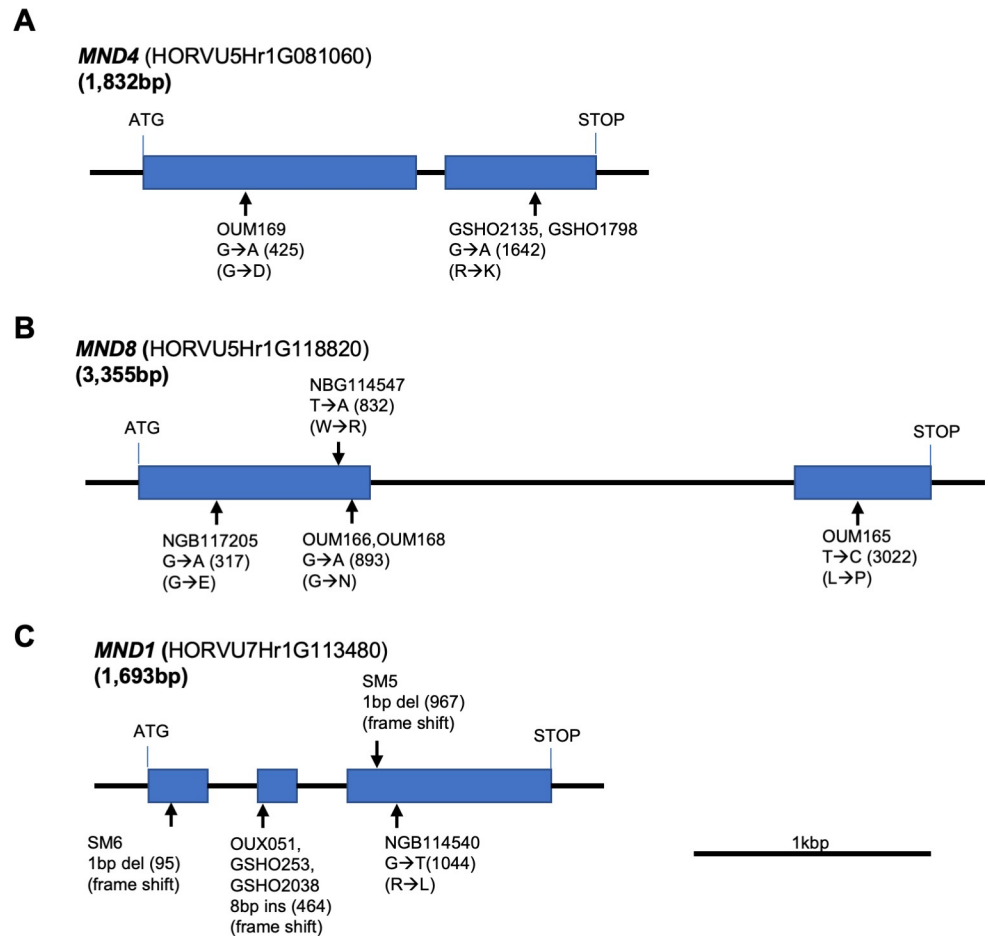


Fig 3. Genomic structure of MND genes. (A–C) Genomic structure and mutation points of MND genes. (A) *MND4*, (B) *MND8*, and (C) *MND1*. Boxes indicate exons, arrows indicate mutation points.

<https://doi.org/10.1371/journal.pgen.1009292.g003>

(S7 and S8 Figs). However, we did not find nucleotide polymorphisms between Akashinriki and the other *mnd* mutants with *mnd1* alleles, i.e., *mnd1*_{GSHO253} and *mnd1*_{SM6}. Based on these inconsistent mapping and sequencing results, *HvPLA3* is not responsible for *mnd1*.

Because it is unlikely that *MND1* and *MND8* are *HvPLA2* or *HvPLA3*, we searched for other candidate genes that regulate the plastochron based on reports in species other than rice. Rough mapping in barley showed that *mnd8* is located 7.2 cM distal to the barley EST marker k08652 (syn. HORVU5Hr1G112990), in the distal region of the long arm of chromosome 5H according to the EST map [31] (S6 Fig). Around the mapped region, we found a candidate gene, a homolog of *BIGE1*, which regulates not only embryo size but also the leaf initiation rate in maize [24]. We subsequently examined the nucleotide sequence of the *BIGE1* homolog (HORVU5Hr1G103900), which encodes a MATE transporter-family protein. We found a T-to-C single base change (T3022C) mutation in the second exon of the gene in *mnd8*_{OUM165} that caused a Leu-to-Pro amino-acid substitution (L404P) (Figs 3B and S9 and Table 1). The nucleotide sequence of the gene in four *mnd* mutants—OUM166, OUM168Ku, NGB114547, and NGB117205—revealed three independent mutations causing amino-acid substitutions (G106E, W278R, and G298N) in the coding region. Accordingly, we concluded that this MATE transporter-like gene is *MND8*. A phylogenetic analysis indicated that *MND8* is an ortholog of maize *BIGE1* (S4 Fig).

Next, we mapped *mnd1* using publicly available simple sequence repeat (SSR) markers in barley [32] (S6 Fig). Barley *mnd1* was located in the distal region of the long arm of barley chromosome 7H, flanked by the barley EST markers, k09432 (syn. HORVU7Hr1G109770) and k04741 (syn. HORVU7Hr1G115050). Using this map information, we searched for *mnd1* candidate genes. We identified as a strong candidate for *MND1* (HORVU7Hr1G113480), a homolog of *HOOKLESS1* (*HLS1*), which encodes an N-acetyltransferase-like protein. Although there are no reports on *HLS1* homologs regulating the plastochron in *Arabidopsis*, multiple *Arabidopsis* mutants of *HLS1* homologs exhibited excess leaf production and a small leaf size [33–35]. One *HLS1* homolog in barley was located near the distal arm region of chromosome 7HL, where *mnd1* was mapped. Sequence analysis of this gene revealed that *mnd1*_{OUX051} carries an eight-nucleotide deletion in the second exon starting at position 464, causing a frameshift and introducing a premature stop codon (Figs 3C and S10 and Table 1). Sequencing of four *mnd* mutants with the *mnd1* alleles (*mnd1*_{SM5}, *mnd1*_{SM6}, *mnd1*_{GSHO253}, and *mnd1*_{GSHO2038}) and one other *mnd* mutant, NGB114540, revealed an eight-base insertion, two independent one-base deletions, and one amino-acid substitution in the coding region (Figs 3C and S10 and Table 1). In addition, among the mutations in *MND1*, the eight-base insertion in *mnd1*_{OUX051}, *mnd1*_{GSHO253}, and *mnd1*_{GSHO2038} was identical to that was recently reported in *mnd1.a* [28]. Therefore, we concluded that this *HLS1*-like gene is *MND1*. A phylogenetic analysis indicated that *MND1* is an ortholog not of *HLS1* but of *GW6a*, a quantitative trait locus that regulates grain weight in rice [36] (S4 Fig).

Accordingly, the three *MND* genes—*MND4*, *MND8*, and *MND1*—encode CYP78A family, MATE transporter-family, and N-acetyltransferase-like proteins, respectively. The *MND8* is newly identified by this study.

Expression pattern of the three *MND* genes

To evaluate their regulation of the plastochron and leaf growth, the transcript accumulation patterns of the three *MND* genes around the shoot apex were investigated using *in situ* hybridization (Fig 4). No signals were detected in longitudinal sections hybridized with sense probes for *MND4*, *MND8* and *MND1* (S11 Fig). *MND4* expression was observed both in the SAM and leaf primordia (Fig 4A). The expression pattern in the SAM was complex, with expression detected in small patches of the SAM flank in the longitudinal sections. One patch was observed at the boundary between the SAM and P1 leaf primordia. Cross sections revealed that the patch corresponded to a semicircular band in the SAM (Fig 4D). Strong *MND4* expression was also observed in the proximal part of the adaxial and abaxial sides of P1–P4 leaf primordia, including the boundary between successive leaf primordia (Fig 4A and 4G). Expression of *MND8* was weak in the SAM and young leaf primordia, and was observed faintly in the young stem (Fig 4B, 4E and 4H).

The expression pattern of *MND1* was similar to that of *MND4*; that is, expression was observed in small patches of the SAM and the proximal part of leaf primordia (Fig 4C). However, the area of expression was different from that of *MND4*. First, *MND1* expression was detected not at the boundary between the SAM and P1 leaf primordia but in the inner region of the SAM (Fig 4C and 4F). Second, gene expression at the boundary between successive leaf primordia was marked for *MND4*, but not for *MND1*. Finally, *MND1* expression in the proximal part of leaf primordia was shifted distally and medially compared to *MND4* (Fig 4C and 4I).

These observations suggest that *MND4* and *MND1* regulate the plastochron and leaf growth by means of their expression in limited but distinct regions of the SAM and leaf primordia.

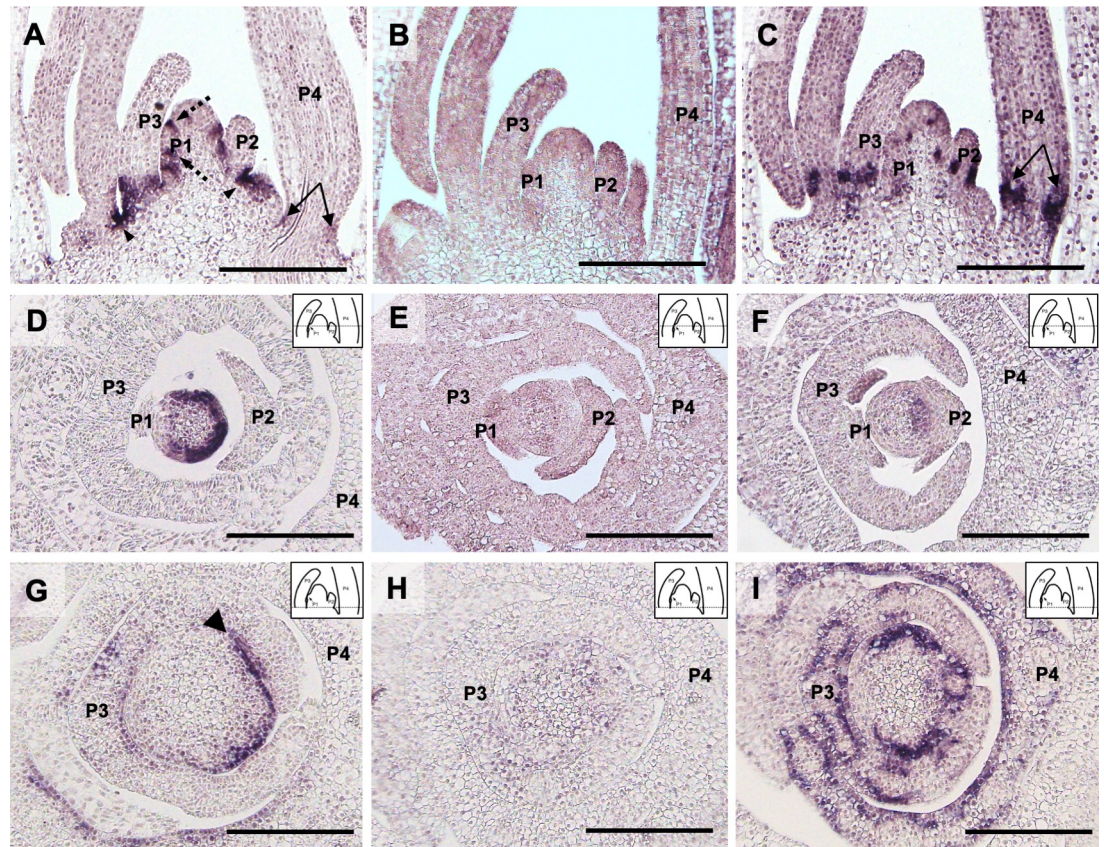


Fig 4. Expression pattern of the three *MND* genes in the shoot apex at 10 days after germination. (A, D, G) *MND4*, (B, E, H) *MND8*, and (C, F, I) *MND1*. The P1–P4 leaf primordia are labeled. Arrowheads in (A) and (G) indicate gene expression at the boundaries between leaf primordia. The dashed arrow in (A) indicates expression at the boundary between the shoot apical meristem and P1 leaf primordium. Two-headed arrows indicate expression at the leaf base. Note the relative position of expression at the leaf base differs between (A) and (C). The dashed line in the inset of D–I corresponds roughly to the position of the section of A–C. Bars: 200 μ m.

<https://doi.org/10.1371/journal.pgen.1009292.g004>

Effect of *mnd* mutations on the expression level of the three *MND* genes

To examine whether *MND* genes regulate other *MND* genes, we compared the expression levels of *MND* genes among three *mnd* mutant backgrounds and WT Akashinriki and Mesa, with the former the original cultivar of *mnd4*_{OUM169} and *mnd8*_{OUM165} and the latter that of *mnd1*_{OUX051} (Fig 5). Quantitative real-time PCR revealed that the expression of *MND8* was slightly decreased in *mnd4*_{OUM169} (Fig 5A). This indicates that *MND4* positively regulates *MND8* expression. The expression level of *MND4* was slightly upregulated in *mnd8*_{OUM165} and significantly upregulated in *mnd1*_{OUX051}, suggesting that *MND1* negatively regulates *MND4* expression (Fig 5B). The expression level of *MND1* was upregulated in *mnd8*_{OUM165} and downregulated in *mnd1*_{OUX051}, implying that *MND8* negatively regulates *MND1* expression and that *mnd1*_{OUX051} affects the accumulation of *MND1* mRNA (Fig 5C). In addition, we examined the expression of *HvPLA2* and *HvPLA3* (Fig 5D and 5E). Although *HvPLA3* expression was not significantly altered in the three *mnd* mutants (Fig 5E), *HvPLA2* expression was downregulated in the *mnd* mutants (Fig 5D). This suggests that the three *MND* genes positively regulate *HvPLA2* expression.

Accordingly, the expression levels of the three *MND* genes in addition to that of *HvPLA2* were affected by functional defects in other *MND* genes.

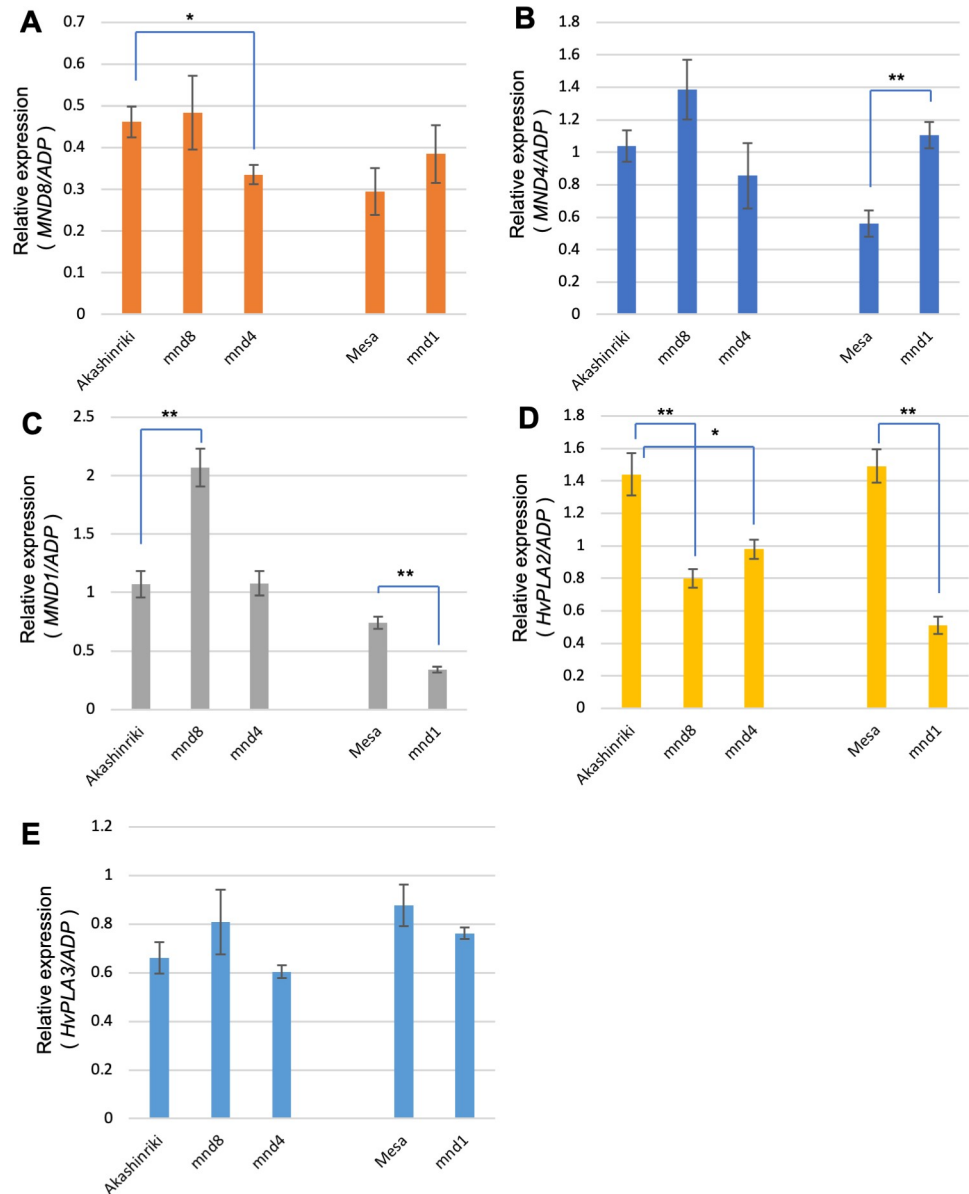


Fig 5. Expression change in *MND* and *HvPLA* in *mnd* mutant backgrounds. Relative expression levels of *MND8* (A), *MND4* (B), *MND1* (C), *HvPLA2* (D), and *HvPLA3* (E) (n = 5). *ADP-ribosylation factor 1-like protein* (*ADP*) was used as the internal control. Double and single asterisks indicate a statistically significant difference compared to the wild type (WT); *t*-test, P < 0.01 and 0.05, respectively).

<https://doi.org/10.1371/journal.pgen.1009292.g005>

Genetic interactions among *MND* genes

To examine the genetic interactions among *MND* genes, we generated double mutants between *mnd8*_{OUM165} and *mnd4*_{OUM169} as well as *mnd8*_{OUM165} and *mnd1*_{OUM051} (Fig 6A and 6B). We measured the leaf number and leaf blade length in the F₃ population at 2 months after germination and determined the genotypes (Fig 6C and 6D). Among the segregants of the F₃ population of *mnd8*_{OUM165} and *mnd4*_{OUM169}, double homozygotic plants for *mnd8*_{OUM165} and *mnd4*_{OUM169} produced the largest number of leaves among the nine genotypes (Fig 6A and 6C). Although the difference in leaf number between single *mnd8*_{OUM165} homozygotic plants

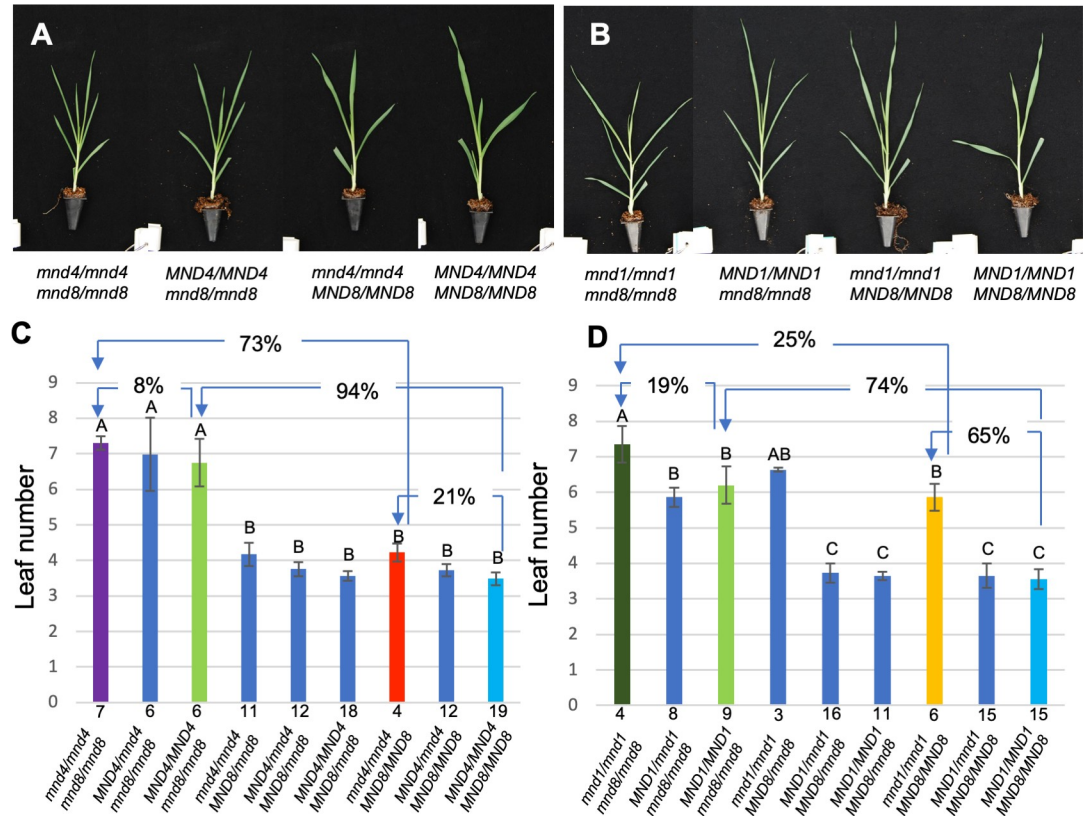


Fig 6. Effect of *mnd* double mutations on leaf number. (A, B) Seedling phenotypes of single and double mutants of *mnd4*_{OUM169} and *mnd1*_{OUX051} (A) and *mnd4*_{OUM169} and *mnd8*_{OUM165} (B) at 2 months after germination. Genotypes are indicated below. (C, D) Effect of *mnd4*_{OUM169} and *mnd1*_{OUX051} (C) as well as *mnd4*_{OUM169} and *mnd8*_{OUM165} (D) alleles on leaf number. Arrows and percentages indicate the effect of homozygotic mutations of *mnd* mutants on the rate of increase in leaf number. Numbers below the columns indicate sample numbers. Different letters above the columns represent significant differences among the genotypes by Tukey-Kramer's test ($P < 0.05$). Values in C and D are means \pm SD.

<https://doi.org/10.1371/journal.pgen.1009292.g006>

and double homozygotic plants was slight, mature double-mutant plants exhibited an enhanced phenotype relative to the *mnd8*_{OUM165} single mutant (S12 Fig), indicating that the *mnd8*_{OUM165} allele has an additive effect with *mnd4*_{OUM169}. Among the segregants of the F₃ population produced from *mnd8*_{OUM165} and *mnd1*_{OUX051}, an additive effect between the two alleles on leaf number was evident; that is, the *mnd8*_{OUM165} *mnd1*_{OUX051} double mutant had the largest number of leaves among the genotypes (Fig 6B and 6D).

The *mnd* alleles had different effects on the increase in leaf number depending on their genotype (Fig 6C and 6D). For example, *mnd8*_{OUM165} increased leaf numbers in the WT and *mnd4*_{OUM169} backgrounds by 94% and 73%, respectively. Similarly, *mnd4*_{OUM169} increased leaf numbers in the WT and *mnd8*_{OUM165} backgrounds by 21% and 8%, respectively (Fig 6C). The same tendency was observed for combinations of *mnd8*_{OUM165} and *mnd1*_{OUX051} (Fig 6D). Accordingly, the effect of a single *mnd* allele on the increase in leaf number was diminished by the accumulation of other *mnd* alleles.

Therefore, *MND8* regulates the plastochron independently of *MND4* and *MND1*. In addition, there are genetic or developmental mechanisms that moderately affect the leaf production rate in the short plastochron background.

Relationship between the plastochron and leaf-blade length in the *mnd* mutant

The shortened plastochron in most plastochron-related mutants is reportedly accompanied by the production of small leaves [4,6,7,24]. However, the correlation between leaf production rate and leaf length is unknown. Therefore, the leaf number at 2 months after germination and the length of the second leaf blade of F₃ segregants produced from *mnd8*_{OUN165} and *mnd4*_{OUN169} and from *mnd8*_{OUN165} and *mnd1*_{OUX051} were measured (Fig 7). A strong negative correlation between leaf number and leaf-blade length was observed in all F₃ segregants for both *mnd8*_{OUN165} and *mnd4*_{OUN169} crosses and *mnd8*_{OUN165} and *mnd1*_{OUX051} crosses (Fig 7A and 7B). This correlation was caused by the strength of the allelic effect on leaf production (Fig 6C and 6D). By contrast, no negative correlations were detected among the most of groups of segregants with identical genotypes (S13 Fig). In addition, among various WT and *mnd* mutant strains, no correlation between leaf number and the maximum length of the leaf blade was observed (S14 Fig and S2 Table).

These observations indicate that the plastochron and leaf-blade length are positively regulated by *MND* genes. However, the correlations between the plastochron and leaf length in the *mnd* mutants were slightly incomplete, suggesting that *MND* may partially acts on pathways that regulate the plastochron and leaf-blade length independently.

Effect of rice *MND* orthologs on plastochron regulation

Our results demonstrated that *MND8* and *MND1* regulate the plastochron in barley, but whether the rice homologs of these genes are involved in plastochron regulation is unknown. Therefore, we constructed knockout mutants of rice *MND8* and *MND1* orthologs using CRISPR/Cas9 (S15 Fig). A phylogenetic analysis indicated that two orthologs of barley *MND8* and *MND1* are present in rice (S4 Fig; two rice orthologs, *OsBE1*/Os03g0839200 and *OsBE2*/Os12g0552600, for barley *MND8* and two rice orthologs, *OsGNAT1*/Os06g0650300 and *OsGNAT2*/Os02g0180400, for barley *MND1*). We generated single and double mutants of the rice orthologs and calculated the plastochron (Fig 8A–8G). The number of leaves increased in *osgnat1*, *osbe1*, *osgnat1 osgnat2*, and *osbe1 osbe2* compared to the WT, but to a lesser extent compared to *pla1-4* (Figs 8G and S16). This indicates that rice *OsBE1* and *OsGNAT1* are involved in plastochron regulation, as are their orthologs in barley, but their contribution to the plastochron is of lesser magnitude than that of *MND* in barley.

In situ hybridization showed that *OsBE1* and *OsGNAT1* were expressed around SAMs, particularly at the base of young leaf primordia (Fig 8H–8M), whereas *OsBE2* and *OsGNAT2* expression was not observed. We next compared the expression patterns of *PLA1*, *OsBE1*, and *OsGNAT1*. Although *PLA1* and *OsBE1* expression domain overlapped, *PLA1*, but not *OsBE1*, was expressed at the base of the P1-related region in the SAM (Fig 8H and 8I). In addition, *OsBE1*, but not *PLA1*, expression was detected in the inner tissue of P3 and the stem tissue (Fig 8K and 8L). *OsGNAT1* expression was strongest at the base of P3 and the boundaries of leaf primordia (Fig 8J and 8M). Expression of the three genes partially overlapped, but none was expressed in the vascular bundle (Fig 8K–8M). By contrast, there were differences in the expression patterns of the rice and barley orthologs, although *MND4* and *PLA1* expression was similar. Punctate expression of *MND1* was observed in the SAM (Fig 4C), whereas *OsGNAT1* expression was detected in the P3 leaf primordium but not in the SAM (Fig 8J and 8M). *MND8* did not exhibit a specific expression pattern (Fig 4B), but *OsBE1* was expressed around the shoot apex (Fig 8I and 8L).

These results indicate functional conservation between the barley and rice orthologous genes (*MND8* versus *OsBE1* and *MND1* versus *OsGNAT1*).

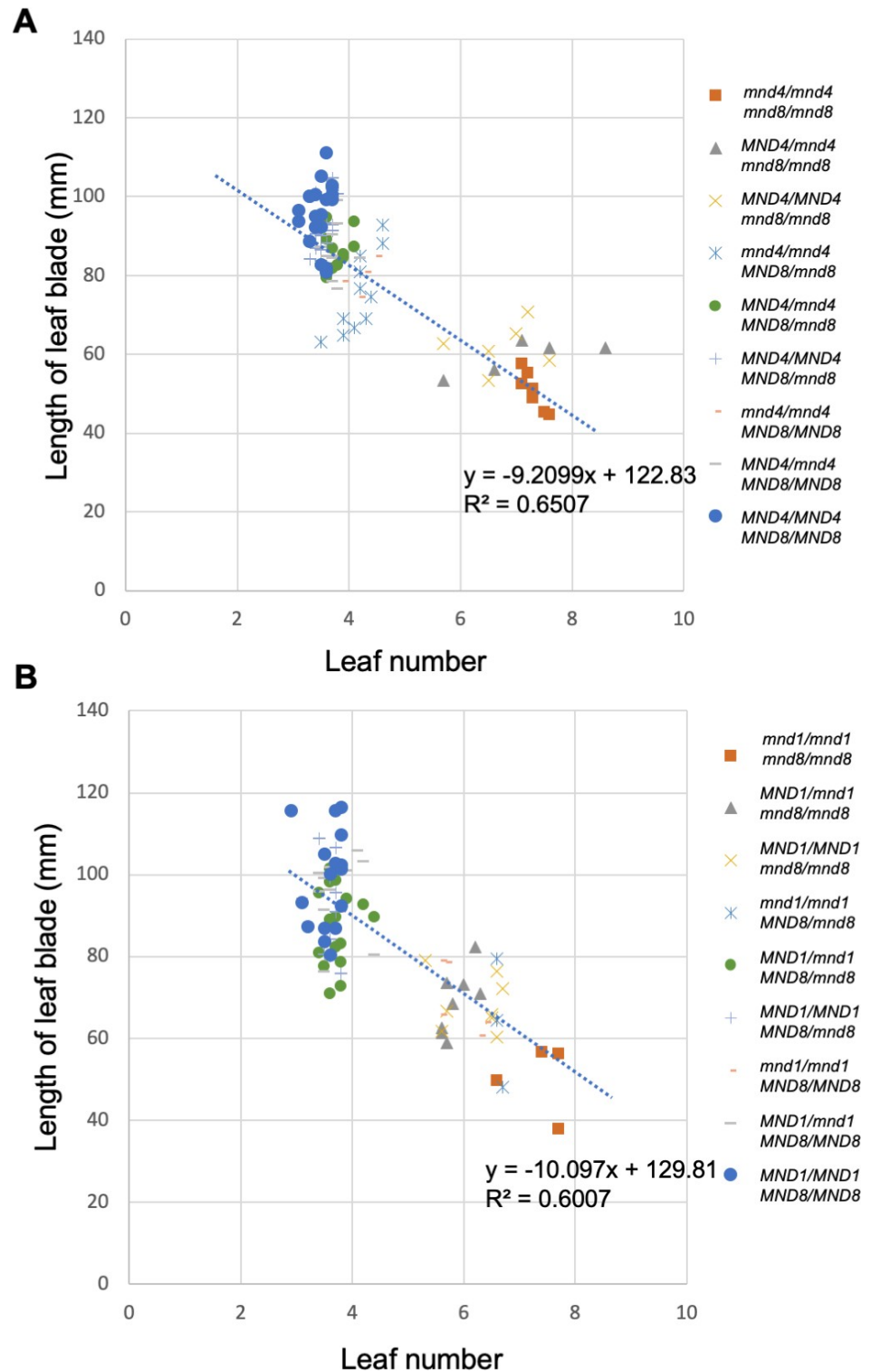


Fig 7. Relationship between leaf number and leaf-blade length. (A, B) Scatter plots of leaf number at 2 months after germination and the length of the second leaf blade in segregated plants from *mnd4*_{OUM169} × *mnd8*_{OUM165} (A) and *mnd1*_{OUM051} × *mnd8*_{OUM165} (B) crossings. The linear regression line and coefficient of determination (R^2) are indicated.

<https://doi.org/10.1371/journal.pgen.1009292.g007>

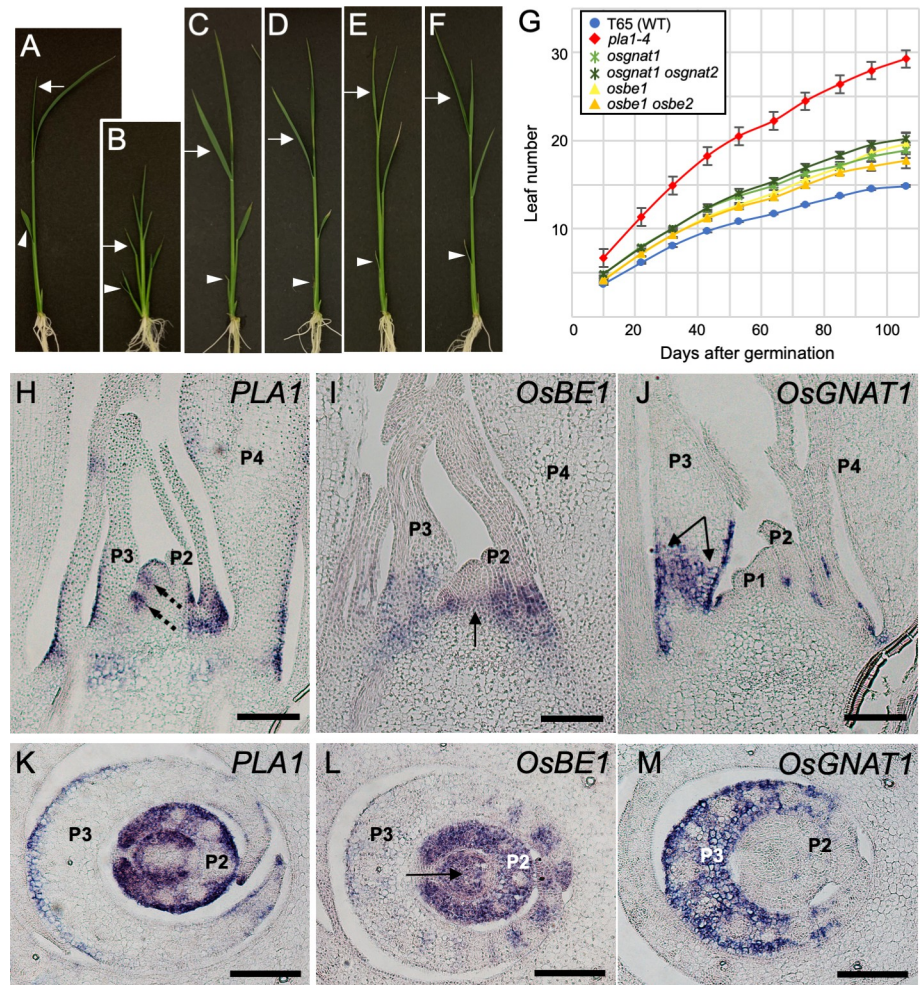


Fig 8. *MND* orthologs in rice. (A–F) Seedlings of the WT and rice mutants in *mnd* orthologs at 10 days after germination. (A) T-65, (B) *pla1-4*, (C) *osbe1*, (D) *osbe1 osbe2*, (E) *osgnat1*, and (F) *osgnat1 osgnat2*. Arrowheads and arrows in (A–F) indicate the second and fourth leaf blades, respectively. (G) Changes in leaf number during vegetative development ($n = 5$). (H–M) Localization of *PLA1* (H, K), *OsBE1* (I, L), and *OsGNAT1* (J, M) mRNAs in longitudinal (H–J) and cross (K–M) sections of the shoot apex of 10-day-old seedlings. The P2–P4 leaf primordia are labeled. The dashed arrows in (H) indicate expression at the boundary between the shoot apical meristem and P1 leaf primordium. The arrows in (I) and (L) indicate expression in the young stem. Two-headed arrow in (J) indicates expression at the leaf base. Bars: 100 μ m.

<https://doi.org/10.1371/journal.pgen.1009292.g008>

Discussion

Three *MND* genes regulate the plastochron via similar developmental pathways, but have unrelated functions and genetic pathways

Our results indicate that the many-noded phenotype of *mnd* mutants results from the rapid production of leaf primordia, which is caused by loss-of-function of three independent genes, *MND4*, *MND8*, and *MND1*. Although the magnitude of the plastochron reduction differed among the mutant alleles, the overall phenotypes of all *mnd* mutants during vegetative development were similar. In addition, the panicle-development phenotypes were comparable among the mutants. Therefore, common abnormalities were exhibited during vegetative and reproductive development, indicating that the three *MND* genes have similar roles in barley development.

Despite their similar biological functions, the three *MND* genes encode unrelated proteins. *MND4* encodes a CYP78A monooxygenase whose substrates are unknown [29]. Although CYP78A genes are important for development in several species [29,37–41], the synthetic or metabolic pathways in which CYP78A is involved are unknown. *MND1* encodes an N-acetyltransferase-like protein and is the closest homolog of *GW6a* in rice [36]. Because *GW6a* exhibits histone H4 acetyltransferase activity, *MND1* also likely regulates the transcription of downstream genes by acetylating histone H4. Furthermore, *MND8* is an ortholog of maize *BIGE1*, a transporter implicated in the secretion of an unidentified small molecule [24]. Accordingly, it is assumed that *MND4*, *MND1*, and *MND8* are involved in the synthesis or metabolism of unknown factors, transcriptional regulation of downstream genes, and transportation of unidentified molecules, respectively. Although a close relationship between the CYP78A pathway and *BIGE1* has been proposed [24], there is no direct evidence that *BIGE1* is associated with the transportation of CYP78A-related molecules so far. In fact, although we did not investigate the relationship between *MND4* and *MND1*, our genetic analysis indicates that *MND4* and *MND1* regulate the plastochron independently of *MND8*. Accordingly, at least two different genetic pathways regulate the plastochron in barley. This is also the case for plastochron regulation by three *PLA* genes in rice. The *pla1*, *pla2*, and *pla3* mutants have a short plastochron and a small leaf size, and conversion of the primary rachis into a shoot occurs in all three, but it has been proposed that *PLA1*, *PLA2*, and *PLA3* regulate the plastochron independently [7,9]. On the other hand, *Arabidopsis* *AMP1* and *CYP78A5/7*, which are orthologs of *PLA3* and *PLA1*, respectively, act on a common downstream process [42].

Therefore, the developmental program controlling leaf initiation, leaf growth, and panicle development in rice and barley is regulated by multiple and independent genetic pathways involving *PLA* and *MND* genes.

Interactions of *MND* genes

At least two independent genetic pathways seem to regulate the plastochron, but complex genetic interactions were also suggested by the expression analysis. In short, *MND8* negatively affects the expression level of *MND1*, *MND1* negatively affects that of *MND4*, and *MND4* positively affects that of *MND8*. It was also noted that *MND4* expression was slightly upregulated, but not significantly, in *mnd8*. Such a regulatory relationship between CYP78A and a *MND8*-related transporter has also been reported in maize; *i.e.*, the expression of some CYP78A family genes was upregulated in the *bige1* mutant background [24]. In maize, *BIGE1* is required for feedback regulation of CYP78A family genes. If this is also the case in barley, the upregulation of *MND4* and *MND1* might have been the result of a deficiency in feedback regulation caused by the loss of *MND8* function. By contrast, overexpression of rice *GW6a*, an ortholog of *MND1*, and the *mnd1.a* mutation affected the expression levels of thousands of genes in rice and barley, respectively [28,36]. Because *GW6a* is predicted to be a transcriptional regulator that modulates chromatin status, a change in *MND4* expression in *mnd1* could be a direct or indirect effect of loss of histone acetyltransferase activity by *MND1*. Although *MND4* and *MND8* do not directly affect gene transcription, they modulate that of other genes by influencing downstream events. In addition to the three *MND* genes, expression of *HvPLA2* was downregulated in the three *mnd* mutants. This indicates that *HvPLA2* is involved in plastochron regulation downstream of the three *MND* genes.

Phenotypic analysis of double mutants revealed that the effect of *MND* genes on plastochron regulation was dependent on the number of *mnd* mutant alleles present. In addition, the increase in leaf number in the double mutants was much less than when the effects of the two mutant alleles on leaf number were equally additive. There are two possible explanations for this phenomenon. One is that genetic pathways regulating plastochron are not completely

independent between *MND8* and *MND4/MND1*. In fact, expression levels of *MND4* and *MND1* were increased in the *mnd8* background, which might weaken the short plastochron phenotype in the single and double mutants. Another is that a developmental restriction would exist, for example, responses of cells (e.g. division activity) in the SAM by the loss of each *MND* function do not proportionally affect leaf production rate. In any case, complex genetic and developmental interactions are implicated in the regulation of the plastochron.

***MND* genes function in leaf production and growth**

In shortened-plastochron mutants, rapid leaf production is accompanied by small leaves [4, 6,7,24]. In *pla1* and *pla2* mutants in rice, a model of the effect of leaf production on leaf size was proposed. According to the model, rapid leaf production by *pla* mutants is not the result of the loss of *PLA* function in the SAM, but an indirect effect of accelerated leaf maturation in leaf primordia [7]. The model was based on the observation that *PLA* genes were expressed in leaf primordia but not in the SAM, although the mechanism by which the change in leaf-primordia maturation affects leaf production is unknown.

Our barley analysis basically supports the above notion. The relative developmental stage and cell-division activity of successive leaf primordia were maintained or increased in the *mnd* mutants. Therefore, leaf production and leaf-primordia maturation were accelerated, as for *pla* mutants in rice. In addition, maize *PLA1* genes control the duration of cell division in the leaf primordia [41], which is consistent with the rapid leaf maturation observed in the *mnd4* mutant in this study. Accordingly, *MND* genes maintain the leaf-maturation schedule. However, if the leaf production rate is affected only by leaf maturation, as suggested by the rice model, the correlation between leaf number and leaf-blade length should be solid. However, we showed that leaf number and leaf-blade length were not always correlated in plants of identical genotype, implying that the plastochron and leaf size are differentially regulated. In fact, expression of *MND4* and *MND1* was observed both in the SAM and leaf primordia. *MND* expression in the SAM may be required for the suppression of leaf initiation independently of expression in the leaf primordia, which is necessary for the suppression of leaf maturation. Based on our findings, we propose a model that not only *MND* function in the leaf primordia but also in the SAM would be important for plastochron regulation in barley. This is supported by the fact that enhanced expression of the maize *PLA1* ortholog in leaf primordia affected leaf size but not leaf number [41], whereas overexpression of *PLA1* via the introduction of an increased gene copies resulted in a prolonged plastochron and an increased leaf size [43].

The mechanisms by which *MND* genes regulate leaf initiation in the SAM and leaf growth in the leaf primordia are unknown. Auxin may be associated with control of the duration of cell-division activity by maize *PLA1* [41]. It is also probable that auxin triggers leaf initiation via *MND*-mediated regulation, because the local auxin concentration is important for leaf initiation in the SAM [1,44]. It is possible that the limited *MND1* and *MND4* expression domain in the SAM is important for the auxin flow or concentration required for proper leaf initiation. Analysis of auxin dynamics in the mutant SAM may provide insight into the role of auxin in the temporal regulation of leaf initiation by *MND* genes.

Conservation and diversity of genetic pathways in rice and barley

Although several genetic factors regulating the plastochron have been identified in rice, maize, *Arabidopsis*, and other species, our understanding of their functional conservation among plant species is inadequate. We characterized *mnd* mutants in barley and identified the responsible genes. It was somewhat surprising that two of the three *MND* genes were not homologs of three *PLA* genes in rice. At least five genes are involved in developmental pathways

underpinning plastochron regulation in grasses. Moreover, three of the five orthologs perform similar functions in rice and barley. However, there was a considerable difference in the magnitude of their effects between the two species. For example, loss-of-function of *MND1* and *MND8* markedly shortened the plastochron in barley, but that of the rice orthologs *OsGNAT1* and *OsBE1* resulted in a slight effect, even for double loss-of-function of closely related paralogs. This might have been caused by differences in genetic redundancy and functional diversification of gene families between the two species. Namely, other homologs in different clades compensate for the function of plastochron regulation in rice. In fact, the functional ortholog of *MND4* in rice is *PLA1*, but it is not the closest homolog among the CYP78A members [29]. It is predicted that *Os09g0528700* is a phylogenetic ortholog of *MND4* in rice, which is specifically expressed in roots and the embryo (<http://ricexpro.dna.affrc.go.jp>), unlike *PLA1*. In terms of the functions of *MND8*-related MATE transporter-family genes, *BIGE1* in maize regulates both the leaf initiation rate and embryo size [24]. However, *mnd8* in barley did not exhibit a phenotype change in terms of embryo size (S17 Fig). In addition, *OsBE1*, a rice ortholog of *MND8*, exhibited specific expression around the shoot apex, unlike *MND8*. Accordingly, the phenotypic effect and expression pattern of the closest homologs of *MND* genes differ among grass species.

Our understanding about a conserved function of plastochron-related genes among grass species is still insufficient. Identifications of *HvPLA2* and *HvPLA3* mutants in barley and comparative analyses with their rice counterparts would advance an understanding of the conservation and diversity of plastochron-related genes.

Materials and methods

Plant materials and growth conditions

The barley *mnd* mutant and WT strains used in this study were listed in Table 1. Mutant and wild-type seeds were sown in soil and the seedlings were transplanted into the pots under conditions in the greenhouse of the University of Tokyo, and the plants were sampled and their phenotypes evaluated at predetermined timepoints (S1 Table). For the double mutant analysis, the genotypes of the F₃ plants were identified using PCR-based genotyping.

The *pla1-4* mutant and WT rice plants were grown on soil or MS medium containing 3% sucrose and 1% agar at 28°C under continuous light. Transgenic plants were grown in a bio-hazard greenhouse with temperatures of 30°C in the daytime and 25°C at night.

Histological and morphological analysis

Samples of the mutant and WT plants were fixed with FAA (formaldehyde:glacial acetic acid:50% ethanol, 2:1:17) for 24 h at 4°C for histological analysis, or with PFA (4% [w/v] paraformaldehyde and 1% Triton X in 0.1 M sodium phosphate buffer) for 48 h at 4°C for *in situ* hybridization. They were then dehydrated in a graded ethanol series, after which the ethanol was substituted with 1-butanol, and the samples were embedded in Paraplast Plus (McCormick Scientific). The samples were sectioned at a thickness of 8 μm using a rotary microtome. The sections were stained with hematoxylin for histological analysis. After staining, the sections were mounted with Poly-Mount (Polysciences, Inc.) and observed under a light microscope.

For scanning electron microscopy, plant materials were fixed in PFA for 24 h and dehydrated in an ascending ethanol series, which was then gradually replaced with 3-methyl-butyl-acetate. Samples were critical-point dried, sputter-coated with platinum, and observed under a scanning electron microscope (S-4800, Hitachi) at an accelerating voltage of 10 kV.

***In situ* hybridization**

Paraffin sections were prepared as described above. For digoxigenin-labeled antisense RNA probes, those for histone *H4* (*HvH4*: HORVU5Hr1G086620), *MND4*, *MND8*, and *MND1* in barley and *OsBE1* and *OsGNAT1* in rice were prepared using cDNAs and specific primers (S3 Table). In addition, antisense RNA probes for *MND4*, *MND8*, and *MND1* were also prepared. The *PLA1* antisense probes were prepared as described previously [5]. *In situ* hybridization and immunological detection using alkaline phosphatase were performed according to the methods of Kouchi and Hata [45]. The experiments were performed using at least five samples per each probe.

For quantification of cell division activity in the P2 and P3 primordia in WT and *mnd* mutants, the number of histone *H4* spots per area of the leaf primordia were calculated using three independent samples of each genotype (S1 Table). Five serial sections in a sample were used for measurements. The area of the leaf primordium was measured with IMAGEJ (<http://rsb.info.nih.gov/ij/>).

Identification of *MND* genes and *PLA2* and *PLA3* orthologs in barley

The nucleotide sequences of *MND4*, *MND8*, *MND1*, *HvPLA2*, and *HvPLA3* in the *mnd* mutants and WT were determined using sequence information from the IPK Barley Blast Server (https://webblast.ipk-gatersleben.de/barley_ibsc/) and Phytozome (<https://phytozome.jgi.doe.gov/>).

For phylogenetic analyses, the amino-acid sequences of *MND4*, *MND8*, and *MND1* homologs in various plant species were obtained from the Phytozome database. The amino-acid alignment was carried out using GENETYX software (Genetyx), and the phylogenetic tree was constructed based on the neighbor-joining method with 1,000-replicate bootstrapping using Molecular Evolutionary Genetics Analysis (MEGA X; [46]).

Quantitative real-time PCR

RNA was extracted from 1 cm of the most basal part of the shoot apices of barley seedlings at 14 DAG using TRIzol reagent (Invitrogen). The extracted RNA was treated with Recombinant DNase I (TaKaRa), and cDNA was synthesized using the High-Capacity cDNA Reverse Transcription Kit (Life Technologies). Quantitative real-time PCR was performed with the StepOne Real-Time PCR System (Life Technologies) using TaqMan Fast Universal PCR Master Mix and FAM-labeled TaqMan probes for each gene. *ADP-ribosylation factor 1-like protein* (*ADP*) was used as the internal standard [47]. In all experiments, we analyzed three technical and five biological replicates (S1 Table). The primers and TaqMan probes for *MND1*, *MND4*, *MND8*, *ADP*, *HvPLA2*, and *HvPLA3* are listed in S4 Table.

Generation of knockout alleles of rice *MND* orthologs using the CRISPR/Cas9 system

The CRISPR/Cas9 system was used to generate knockout alleles for *OsBE1*, *OsBE2*, *OsGNAT1*, and *OsGNAT2*, which are orthologs of *MND1* and *MND8* in rice. The target sites were selected using the CRISPR-P program (<http://cbi.hzau.edu.cn/crispr/>) [48] (S15 Fig). The single-guide RNA (sgRNA) cloning vector (pZK_gRNA) and all-in-one binary vector (pZH_OsU6gRNA_MM Cas9) harboring sgRNA, Cas9, and NPTII were provided by Masaki Endo [49]. The pZH_OsU6gRNA_MM Cas9 vector including target-guide RNA for *MND* orthologs was constructed as described previously [49].

The constructs were introduced into *Agrobacterium tumefaciens* strain EHA105 and transformed into cultivar Taichung-65 (T-65) calli via *Agrobacterium*-mediated transformation. Mutations and transgenes in each transformant were confirmed by sequencing and PCR-based detection (S15 Fig).

We performed rough observations of morphological phenotypes with at least three or more loss-of-function alleles. And then, we used only transgene-free genome edited plants (null segregants) for each gene for analyzing in detail and generating double mutants in our experiments.

Supporting information

S1 Fig. Changes in the leaf primordia of *mnd* mutants at 1–2 weeks after germination.

Inner structure of the wild-type and *mnd* mutants at 1 week (A–D) and 2 weeks (E–H) after germination. (A, E) Akashinriki, (B, F) *mnd8*_{OUM165}, (C, G) *mnd4*_{OUM169}, and (D, H) *mnd1*_{OUX051}. xL indicates the xth leaf and Px indicates the order of leaf emergence from the shoot apical meristem. col, coleoptile. Bars: 200 μ m.

(TIF)

S2 Fig. Panicle phenotypes of *mnd* mutants. Arrows indicate elongated bracts or ectopic shoot-like structures; arrowheads indicate branched panicles.

(TIF)

S3 Fig. Quantification of the *H4* signals in *mnd* mutants. (A, B) The number of histone *H4* spots per area of the leaf primordia were calculated using three independent samples of each genotype by *in situ* hybridization. (A) P2, (B) P3. Five serial sections in a sample were used for measurements. Data are shown as mean \pm SD. The area of the leaf primordium was measured with IMAGEJ (<http://rsb.info.nih.gov/ij/>). ***P* < 0.01 (Student's *t*-test).

(TIF)

S4 Fig. Phylogenetic tree of MND proteins. Phylogenetic tree of MND proteins from several angiosperms. (A) MND4, (B) MND8, and (C) MND1. Numbers above the branches are bootstrap values from 1,000 replicates. At, *Arabidopsis thaliana*; Zm, *Zea mays*; Os, *Oryza sativa*; Hv, *Hordeum vulgare*. Red and blue underlining indicates MND genes in barley and orthologs in rice, respectively.

(TIF)

S5 Fig. Amino-acid alignment of MND4 and its homologs. Alignment of MND4 and its homologous proteins in several angiosperms used in S4 Fig. The effect of each *mnd* mutation is indicated in red. Black and gray and more than 50% identical amino acids, respectively. At, *Arabidopsis thaliana*; Zm, *Zea mays*; Os, *Oryza sativa*; Hv, *Hordeum vulgare*

(TIF)

S6 Fig. Map position of MND8 and MND1. (A) For genetic mapping of MND8, 21 recessive homozygous F₂ plants from a cross between Haruna Nijo and OUM165 were used. (B) For genetic mapping of MND1, 33 recessive homozygous F₂ plants from a cross between OUI026 and SM6 were used. The double-ended arrows indicate the gene regions found in the mapping. EST markers with initial letter k were those reported by Sato et al. (2009). SSR markers underlined were developed by Varshney et al. (2007). MapMaker version 2.0 was used for map construction with LOD score 3.

(TIF)

S7 Fig. Genomic structure of *HvPLA2* and *HvPLA3*. Boxes indicate exons. DNA polymorphisms between Akashinriki and OUX051 in the *HvPLA3* genomic structure are indicated by arrows.

(TIF)

S8 Fig. Amino-acid alignment of *HvPLA3* and its homologs. Alignment of *HvPLA3* and its homologs in several angiosperms. The effects of mutations in OUX051 are indicated in red. Black and gray, 100% and more than 50% identical amino acids, respectively. LOC, *Oryza sativa*; GRMZM, *Zea mays*; Solyc, *Solanum lycopersicum*; Medtr, *Medicago truncatula*; AT, *Arabidopsis thaliana*.

(TIF)

S9 Fig. Amino-acid alignment of *MND8* and its homologs. Alignment of *MND8* and its homologous proteins in several angiosperms used in S4 Fig. The effect of each *mnd* mutation is indicated in red. Black and gray, 100% and more than 50% identical amino acids, respectively. At, *Arabidopsis thaliana*; Zm, *Zea mays*; Os, *Oryza sativa*; Hv, *Hordeum vulgare*.

(TIF)

S10 Fig. Amino-acid alignment of *MND1* and its homologs. Alignment of *MND1* and its homologs in the angiosperms used in S4 Fig. The effect of each *mnd* mutation is indicated in red. Black and gray, 100% and more than 50% identical amino acids, respectively. At, *Arabidopsis thaliana*; Zm, *Zea mays*; Os, *Oryza sativa*; Hv, *Hordeum vulgare*.

(TIF)

S11 Fig. *In situ* hybridization using sense probes for three *MND* genes. Shoot samples at 10 days after germination were used. (A) *MND4*, (B) *MND8*, and (C) *MND1*. Bars: 200 μ m.

(TIF)

S12 Fig. Mature plant phenotypes of *mnd* double mutants. (A) Segregated plants of the F₃ population derived from the F₂ seeds of *mnd4*_{OUM169} \times *mnd8*_{OUM165} crossings. (B) Segregated plants of the F₃ population derived from the F₂ seeds of *mnd1*_{OUX051} \times *mnd8*_{OUM165} crossings. The genotypes of the plants are indicated.

(TIF)

S13 Fig. Relationship between leaf number and leaf-blade length among plants of the same genotype. (A, B) Scatter plots of leaf number at 2 months after germination and the length of the second leaf blade with the same genotype from *mnd4*_{OUM169} \times *mnd8*_{OUM165} (A), and *mnd1*_{OUX051} \times *mnd8*_{OUM165} (B) crossings. The linear regression line and the coefficient of determination (R^2) are indicated.

(TIF)

S14 Fig. Relationship between leaf number and maximum leaf-blade length. Scatter plot of leaf number at 100 days after germination and the maximum length of the leaf blade. Average values of the traits of five plants were used. The linear regression line and coefficient of determination (R^2) are indicated.

(TIF)

S15 Fig. CRISPR/Cas9-mediated mutagenesis of rice *MND* orthologs. (A–D) Genomic structures and target sites of rice *MND* orthologs. (A) *OsGNAT1*, (B) *OsGNAT2*, (C) *OsBE1*, and (D) *OsBE2*. Boxes indicate exons. Arrows indicate target sites (protospacer adjacent motif [PAM] sequences [red characters] and guide sequences [blue characters]) and directions starting from each PAM sequence. The lower sequence is that of the mutant used in the

experiment. Bars: 500 bp.
(TIF)

S16 Fig. Leaf number of wild-type (T-65) plants and CRISPR/Cas9-induced mutants at 10 days after sowing. Data are presented as the means \pm SDs ($n \geq 5$).
(TIF)

S17 Fig. Seed phenotypes of *mnd* mutants. (A) Akashinriki, (B) *mnd4*_{OUM169}, (C) *mnd8*_{OUM165}, and (D) *mnd1*_{OUX051}. Bars: 2 mm.
(TIF)

S1 Table. Raw data for figures and tables.
(XLSX)

S2 Table. Leaf number and leaf size in the wild type and *mnd* mutants.
(PPTX)

S3 Table. Primers used to produce *in situ* hybridization probes.
(PPTX)

S4 Table. Primers and TaqMan probes used for real-time PCR.
(PPTX)

Acknowledgments

The barley resources were provided by the National Bioresource Project-Barley, Okayama University, Japan; USDA, Aberdeen, Idaho; Nordic Genetic Resource Center, Sweden; and Tochigi Agricultural Experiment Station, Japan.

Author Contributions

Conceptualization: Ken-ichiro Hibara, Takanori Yoshikawa, Masaharu Suzuki, Makoto Kusaba, Shin Taketa, Jun-ichi Itoh.

Data curation: Ken-ichiro Hibara, Jun-ichi Itoh.

Formal analysis: Ken-ichiro Hibara, Jun-ichi Itoh.

Funding acquisition: Jun-ichi Itoh.

Investigation: Ken-ichiro Hibara, Masayuki Miya, Sean Akira Benvenuto, Naoko Hibara-Matsuo, Manaki Mimura, Shin Taketa, Jun-ichi Itoh.

Methodology: Ken-ichiro Hibara, Jun-ichi Itoh.

Project administration: Takanori Yoshikawa, Shin Taketa, Jun-ichi Itoh.

Resources: Ken-ichiro Hibara, Shin Taketa.

Supervision: Ken-ichiro Hibara, Takanori Yoshikawa, Masaharu Suzuki, Makoto Kusaba, Shin Taketa, Jun-ichi Itoh.

Validation: Ken-ichiro Hibara, Masayuki Miya, Shin Taketa, Jun-ichi Itoh.

Visualization: Ken-ichiro Hibara, Jun-ichi Itoh.

Writing – original draft: Ken-ichiro Hibara, Jun-ichi Itoh.

Writing – review & editing: Ken-ichiro Hibara, Masaharu Suzuki, Makoto Kusaba, Shin Taketa, Jun-ichi Itoh.

References

1. Lee B, Yu S, Jackson D. Control of plant architecture: The role of phyllotaxy and plastochron. *J Plant Biol.* 2009; 52(4):277–82. Available from: <http://link.springer.com/10.1007/s12374-009-9034-x>
2. Wang B, Smith SM, Li J. Genetic regulation of shoot architecture. *Annu Rev Plant Biol.* 2018; 69(1):437–68. Available from: <http://www.annualreviews.org/doi/10.1146/annurev-arplant-042817-040422>
3. Itoh J, Hibara K, Kojima M, Sakakibara H, Nagato Y. Rice DECUSSATE controls phyllotaxy by affecting the cytokinin signaling pathway. *Plant J.* 2012; 72(6):869–81. Available from: <https://doi.org/10.1111/j.1365-3113X.2012.05123.x> PMID: 22889403
4. Itoh J-I, Hasegawa A, Kitano H, Nagato Y. A recessive heterochronic mutation, *plastochron1*, shortens the plastochron and elongates the vegetative phase in rice. *Plant Cell.* 1998; 10(9):1511–21. Available from: <http://www.plantcell.org/lookup/doi/10.1105/tpc.10.9.1511> PMID: 9724697
5. Miyoshi K, Ahn B-O, Kawakatsu T, Ito Y, Itoh J-I, Nagato Y, et al. PLASTOCHRON1, a timekeeper of leaf initiation in rice, encodes cytochrome P450. *Proc Natl Acad Sci U S A.* 2004; 101(3):875–80. Available from: <http://www.pnas.org/cgi/doi/10.1073/pnas.2636936100> PMID: 14711998
6. Wang JW, Schwab R, Czech B, Mica E, Weigel D. Dual effects of miR156-targeted SPL genes and CYP78A5/KLUH on plastochron length and organ size in *Arabidopsis thaliana*. *Plant Cell.* 2008; 20(5):1231–43. Available from: <http://www.plantcell.org/content/20/5/1231> PMID: 18492871
7. Kawakatsu T, Itoh J-I, Miyoshi K, Kurata N, Alvarez N, Veit B, et al. PLASTOCHRON2 regulates leaf initiation and maturation in rice. *Plant Cell.* 2006; 18(3):612–25. Available from: <http://www.plantcell.org/lookup/doi/10.1105/tpc.105.037622> PMID: 16461585
8. Veit B, Briggs SP, Schmidt RJ, Yanofsky MF, Hake S. Regulation of leaf initiation by the terminal ear 1 gene of maize. *Nature.* 1998; 393(6681):166–8. Available from: <http://www.nature.com/articles/30239> PMID: 9603518
9. Kawakatsu T, Taramino G, Itoh J-I, Allen J, Sato Y, Hong S-K, et al. PLASTOCHRON3/GOLIATH encodes a glutamate carboxypeptidase required for proper development in rice. *Plant J.* 2009; 58(6):1028–40. Available from: <http://doi.wiley.com/10.1111/j.1365-3113X.2009.03841.x> PMID: 19228340
10. Helliwell CA, Chin-Atkins AN, Wilson IW, Chapple R, Dennis ES, Chaudhury A. The *Arabidopsis* AMP1 gene encodes a putative glutamate carboxypeptidase. *Plant Cell.* 2001; 13(9):2115–25. Available from: <http://www.plantcell.org/lookup/doi/10.1105/TPC.010146> PMID: 11549767
11. Suzuki M, Latshaw S, Sato Y, Settles AM, Koch KE, Hannah LC, et al. The maize viviparous8 locus, encoding a putative ALTERED MERISTEM PROGRAM1-like peptidase, regulates abscisic acid accumulation and coordinates embryo and endosperm development. *Plant Physiol.* 2008; 146(3):1193–206. Available from: <http://www.plantphysiol.org/lookup/doi/10.1104/pp.107.114108> PMID: 18203869
12. Rhoades MW, Reinhart BJ, Lim LP, Burge CB, Bartel B, Bartel DP. Prediction of plant microRNA targets. *Cell.* 2002; 110(4):513–20. Available from: <https://linkinghub.elsevier.com/retrieve/pii/S0092867402008632> [https://doi.org/10.1016/S0092-8674\(02\)00863-2](https://doi.org/10.1016/S0092-8674(02)00863-2) PMID: 12202040
13. Yamasaki K, Kigawa T, Inoue M, Tateno M, Yamasaki T, Yabuki T, et al. A novel zinc-binding motif revealed by solution structures of DNA-binding domains of *Arabidopsis* SBP-family transcription factors. *J Mol Biol.* 2004; 337(1):49–63. Available from: <https://linkinghub.elsevier.com/retrieve/pii/S0022283604000610> <https://doi.org/10.1016/j.jmb.2004.01.015> PMID: 15001351
14. Xie K, Wu C, Xiong L. Genomic organization, differential expression, and interaction of SQUAMOSA promoter-binding-like transcription factors and microRNA156 in rice. *Plant Physiol.* 2006; 142(1):280–93. Available from: <http://www.plantphysiol.org/lookup/doi/10.1104/pp.106.084475> PMID: 16861571
15. Xie K, Shen J, Hou X, Yao J, Li X, Xiao J, et al. Gradual increase of miR156 regulates temporal expression changes of numerous genes during leaf development in rice. *Plant Physiol.* 2012; 158(3):1382–94. Available from: <https://doi.org/10.1104/pp.111.190488> PMID: 22271747
16. Schwarz S, Grande A V., Bujdoso N, Saedler H, Huijser P. The microRNA regulated SBP-box genes SPL9 and SPL15 control shoot maturation in *Arabidopsis*. *Plant Mol Biol.* 2008; 67(1–2):183–95. Available from: <http://link.springer.com/10.1007/s11103-008-9310-z> PMID: 18278578
17. Chuck G, Cigan AM, Saetern K, Hake S. The heterochronic maize mutant *Corngrass1* results from overexpression of a tandem microRNA. *Nat Genet.* 2007; 39(4):544–9. Available from: <http://www.nature.com/articles/ng2001> <https://doi.org/10.1038/ng2001> PMID: 17369828
18. Chuck G, Whipple C, Jackson D, Hake S. The maize SBP-box transcription factor encoded by *tassel-sheath4* regulates bract development and the establishment of meristem boundaries. *Development.* 2010; 137(8):1243–50. Available from: <http://dev.biologists.org/cgi/doi/10.1242/dev.048348> PMID: 20223762
19. Chuck GS, Brown PJ, Meeley R, Hake S. Maize SBP-box transcription factors *unbranched2* and *unbranched3* affect yield traits by regulating the rate of lateral primordia initiation. *Proc Natl Acad Sci U*

- S A. 2014; 111(52):18775–80. Available from: <http://www.pnas.org/lookup/doi/10.1073/pnas.1407401112> PMID: 25512525
20. Jiao Y, Wang Y, Xue D, Wang J, Yan M, Liu G, et al. Regulation of OsSPL14 by OsmiR156 defines ideal plant architecture in rice. *Nat Genet.* 2010; 42(6):541–4. Available from: <http://www.nature.com/articles/ng.591> <https://doi.org/10.1038/ng.591> PMID: 20495565
 21. Miura K, Ikeda M, Matsubara A, Song X-J, Ito M, Asano K, et al. OsSPL14 promotes panicle branching and higher grain productivity in rice. *Nat Genet.* 2010; 42(6):545–9. Available from: <http://www.nature.com/articles/ng.592> <https://doi.org/10.1038/ng.592> PMID: 20495564
 22. Luo L, Li W, Miura K, Ashikari M, Kyozyuka J. Control of tiller growth of rice by OsSPL14 and strigolactones, which work in two independent pathways. *Plant Cell Physiol.* 2012; 53(10):1793–801. Available from: <https://academic.oup.com/pcp/article-lookup/doi/10.1093/pcp/pcs122> PMID: 22960246
 23. Wang L, Sun S, Jin J, Fu D, Yang X, Weng X, et al. Coordinated regulation of vegetative and reproductive branching in rice. *Proc Natl Acad Sci U S A.* 2015; 112(50):15504–9. Available from: <http://www.pnas.org/lookup/doi/10.1073/pnas.1521949112> PMID: 26631749
 24. Suzuki M, Sato Y, Wu S, Kang B-H, McCarty DR. Conserved functions of the MATE transporter BIG EMBRYO1 in regulation of lateral organ size and initiation rate. *Plant Cell.* 2015; 27(8):2288–300. Available from: <http://www.plantcell.org/lookup/doi/10.1105/tpc.15.00290> PMID: 26276834
 25. Druka A, Franckowiak J, Lundqvist U, Bonar N, Alexander J, Houston K, et al. Genetic dissection of barley morphology and development. *Plant Physiol.* 2011; 155(2):617–27. Available from: <http://www.plantphysiol.org/lookup/doi/10.1104/pp.110.166249> PMID: 21088227
 26. Mascher M, Gundlach H, Himmelbach A, Beier S, Twardziok SO, Wicker T, et al. A chromosome conformation capture ordered sequence of the barley genome. *Nature.* 2017; 544(7651):427–33. Available from: <http://www.nature.com/articles/nature22043> <https://doi.org/10.1038/nature22043> PMID: 28447635
 27. Harlan H V., Pope MN. MANY-NODED DWARF BARLEY. *J Hered.* 1922; 13(6):269–73. Available from: <https://academic.oup.com/jhered/article/766940/MANY-NODED>
 28. Walla A, Wilma van Esse G, Kirschner GK, Guo G, Brünje A, Finkemeier I, et al. An acyl-CoA N-acyltransferase regulates meristem phase change and plant architecture in barley. *Plant Physiol.* 2020; 183(3):1088–109. Available from: <http://www.plantphysiol.org/lookup/doi/10.1104/pp.20.00087> PMID: 32376761
 29. Mascher M, Jost M, Kuon J-E, Himmelbach A, Bßalg A, Beier S, et al. Mapping-by-sequencing accelerates forward genetics in barley. *Genome Biol.* 2014; 15(6):R78. Available from: <http://genomebiology.biomedcentral.com/articles/10.1186/gb-2014-15-6-r78> PMID: 24917130
 30. McMaster GS. Phytomers, phyllochrons, phenology and temperate cereal development. *J Agric Sci.* 2005; 143(2–3):137–50. Available from: https://www.cambridge.org/core/product/identifier/S0021859605005083/type/journal_article
 31. Sato K, Nankaku N, Takeda K. A high-density transcript linkage map of barley derived from a single population. *Heredity.* 2009; 103(2):110–7. Available from: <http://www.nature.com/articles/hdy200957> <https://doi.org/10.1038/hdy.2009.57> PMID: 19455180
 32. Varshney RK, Marcel TC, Ramsay L, Russell J, Röder MS, Stein N, et al. A high density barley microsatellite consensus map with 775 SSR loci. *Theor Appl Genet.* 2007; 114(6):1091–103. Available from: <http://link.springer.com/10.1007/s00122-007-0503-7> PMID: 17345060
 33. Lehman A, Black R, Ecker JR. HOOKLESS1, an ethylene response gene, is required for differential cell elongation in the *Arabidopsis* hypocotyl. *Cell.* 1996; 85(2):183–94. Available from: <https://linkinghub.elsevier.com/retrieve/pii/S0092867400810958> [https://doi.org/10.1016/s0092-8674\(00\)81095-8](https://doi.org/10.1016/s0092-8674(00)81095-8) PMID: 8612271
 34. Li H, Johnson P, Stepanova A, Alonso JM, Ecker JR. Convergence of signaling pathways in the control of differential cell growth in *Arabidopsis*. *Dev Cell.* 2004; 7(2):193–204. Available from: <https://linkinghub.elsevier.com/retrieve/pii/S1534580704002175> <https://doi.org/10.1016/j.devcel.2004.07.002> PMID: 15296716
 35. Chang KN, Zhong S, Weirauch MT, Hon G, Pelizzola M, Li H, et al. Temporal transcriptional response to ethylene gas drives growth hormone cross-regulation in *Arabidopsis*. *Elife.* 2013; 2: e00675. Available from: <https://elifesciences.org/articles/00675> <https://doi.org/10.7554/eLife.00675> PMID: 23795294
 36. Song XJ, Kuroha T, Ayano M, Furuta T, Nagai K, Komeda N, et al. Rare allele of a previously unidentified histone H4 acetyltransferase enhances grain weight, yield, and plant biomass in rice. *Proc Natl Acad Sci U S A.* 2015; 112(1):76–81. Available from: <http://www.pnas.org/lookup/doi/10.1073/pnas.1421127112> PMID: 25535376
 37. Anastasiou E, Kenz S, Gerstung M, MacLean D, Timmer J, Fleck C, et al. Control of plant organ size by KLUH/CYP78A5-dependent intercellular signaling. *Dev Cell.* 2007; 13(6):843–56. Available from:

- <https://linkinghub.elsevier.com/retrieve/pii/S1534580707003796> <https://doi.org/10.1016/j.devcel.2007.10.001> PMID: 18061566
38. Chakrabarti M, Zhang N, Sauvage C, Munos S, Blanca J, Canizares J, et al. A cytochrome P450 regulates a domestication trait in cultivated tomato. *Proc Natl Acad Sci U S A*. 2013; 110(42):17125–30. Available from: <http://www.pnas.org/cgi/doi/10.1073/pnas.1307313110> PMID: 24082112
 39. Ma M, Wang Q, Li Z, Cheng H, Li Z, Liu X, et al. Expression of TaCYP78A3, a gene encoding cytochrome P450 CYP78A3 protein in wheat (*Triticum aestivum* L.), affects seed size. *Plant J*. 2015; 83(2):312–25. Available from: <http://doi.wiley.com/10.1111/tpj.12896> PMID: 26043144
 40. Ma M, Zhao H, Li Z, Hu S, Song W, Liu X. Retracted: TaCYP78A5 regulates seed size in wheat (*Triticum aestivum*). *J Exp Bot*. 2016; 67(5):1397–410. Available from: <https://academic.oup.com/jxb/article/67/5/1397/2885115> <https://doi.org/10.1093/jxb/erv542> PMID: 26712825
 41. Sun X, Cahill J, Van Hautegeem T, Feys K, Whipple C, Novák O, et al. Altered expression of maize PLASTOCHRON1 enhances biomass and seed yield by extending cell division duration. *Nat Commun*. 2017; 8(1):14752. Available from: <http://www.nature.com/articles/ncomms14752> <https://doi.org/10.1038/ncomms14752> PMID: 28300078
 42. Poretska O, Yang S, Pitorre D, Poppenberger B, Sieberer T. AMP1 and CYP78A5/7 act through a common pathway to govern cell fate maintenance in *Arabidopsis thaliana*. *PLoS Genet*. 2020; 16(9):1–28. Available from: <http://dx.doi.org/10.1371/journal.pgen.1009043> PMID: 32960882
 43. Hibara K, Isono M, Mimura M, Sentoku N, Kojima M, Sakakibara H, et al. Jasmonate regulates juvenile-to-adult phase transition in rice. *Development*. 2016; 143(18):3407–16. Available from: <http://dev.biologists.org/lookup/doi/10.1242/dev.138602> PMID: 27578792
 44. Reinhardt D, Pesce E-R, Stieger P, Mandel T, Baltensperger K, Bennett M, et al. Regulation of phyllotaxis by polar auxin transport. *Nature*. 2003; 426(6964):255–60. Available from: <http://www.nature.com/articles/nature02081> <https://doi.org/10.1038/nature02081> PMID: 14628043
 45. Kouchi H, Hata S. Isolation and characterization of novel nodulin cDNAs representing genes expressed at early stages of soybean nodule development. *Mol Gen Genet*. 1993; 238–238(1–2):106–19. Available from: <http://link.springer.com/10.1007/BF00279537> PMID: 7683079
 46. Kumar S, Stecher G, Li M, Knyaz C, Tamura K. MEGA X: Molecular evolutionary genetics analysis across computing platforms. *Mol Biol Evol*. 2018; 35(6):1547–9. Available from: <https://academic.oup.com/mbe/article/35/6/1547/4990887> <https://doi.org/10.1093/molbev/msy096> PMID: 29722887
 47. Ferdous J, Li Y, Reid N, Langridge P, Shi B-J, Tricker PJ. Identification of reference genes for quantitative expression analysis of microRNAs and mRNAs in barley under various stress conditions. *PLoS One*. 2015; 10(3):e0118503. Available from: <https://dx.plos.org/10.1371/journal.pone.0118503> PMID: 25793505
 48. Lei Y, Lu L, Liu H-Y, Li S, Xing F, Chen L-L. CRISPR-P: A web tool for synthetic single-guide RNA design of CRISPR-system in plants. *Mol Plant*. 2014; 7(9):1494–6. Available from: <https://linkinghub.elsevier.com/retrieve/pii/S1674205214609527> <https://doi.org/10.1093/mp/ssu044> PMID: 24719468
 49. Mikami M, Toki S, Endo M. Comparison of CRISPR/Cas9 expression constructs for efficient targeted mutagenesis in rice. *Plant Mol Biol*. 2015 19; 88(6):561–72. Available from: <https://link.springer.com/article/10.1007/s11103-015-0342-x> PMID: 26188471